2011-07-06

Characterization of the Mechanical Response of the Lumbar Spine

Shannon Alisa Zirbel
Brigham Young University - Provo

Characterization of the Mechanical Response of the Lumbar Spine

Shannon A. Zirbel

A thesis submitted to the faculty of
Brigham Young University
in partial fulfillment of the requirements for the degree of

Master of Science

Larry L. Howell, Chair
Anton E. Bowden
Brian D. Jensen

Department of Mechanical Engineering

Brigham Young University

August 2011

ABSTRACT

Characterization of the Mechanical Response of the Lumbar Spine

Shannon A. Zirbel
Department of Mechanical Engineering, BYU
Master of Science

The primary objective of this research is to associate lumbar segmental mechanical response with intervertebral disc degeneration under physiologic testing conditions. Because no mathematical model exists for lumbar spine segmental rotations, a portion of this thesis evaluates potential methods for curve fitting the torque-rotation curves. The Dual Inflection Point (DIP) Boltzmann equation was developed during the course of this research and is presented here as a method for fitting spinal motion data wherein a physical meaning can be assigned to each of the model coefficients. This model can tell us more about the effects of degeneration, testing conditions, and other factors that are expressed in the change in spinal motion.

Previous studies have investigated the relationship between the degeneration grade and flexibility of the intervertebral disc, but were completed without the presence of a compressive follower load. This study builds on past work by performing the testing under a compressive follower load. Segmental stiffness, range of motion (ROM), hysteresis area, and normalized hysteresis (hysteresis area/ROM) were evaluated and the effect of degeneration, segment level, temperature, and follower load were analyzed.

Twenty-one functional spinal units (FSUs) were tested in the three primary modes of loading at both body temperature (39 ± 2 °C) and room temperature (21 ± 1 °C) in a near 100% humidity environment. A compressive follower load of 440 N was applied to simulate physiologic conditions. Fifteen of the twenty-one segments were also tested without the follower load to determine the effects of the load on segmental biomechanics. The grade of degeneration for each segment was determined using the Thompson scale and the torque-rotation curves were fit with the DIP-Boltzmann sigmoid curve.

The effect of degeneration was statistically significant ($\alpha = 0.05$) for stiffness, ROM, and hysteresis area in axial rotation (AR) and lateral bending (LB); it was also statistically significant for ROM and normalized hystersis in flexion-extension (FE). The lumbosacral joint (L5-S1) was significantly stiffer in AR and LB; the decrease in ROM and hysteresis area in AR and LB were also statistically significant for the lumbosacral joint compared to L1-L2 and L3-L4. Temperature had a significant effect on stiffness and hysteresis area in AR and on hysteresis area in LB. The follower load increased stiffness in all three modes of loading, but was significant only in AR and LB; it also reduced ROM and increased normalized hysteresis in all three modes of loading.

Keywords: spinal biomechanics, quality of motion, Boltzmann sigmoid, lumbar spine, disc degeneration, torque-rotation response

ACKNOWLEDGMENTS

I would like to first express thanks to the members of my graduate committee, Dr. Howell, Dr. Bowden, and Dr. Jensen, for their mentoring and guidance during this thesis work. I also am grateful for the support of lab members in the Compliant Mechanisms Research group and the BYU Applied Biomechanics Engineering Laboratory. I especially thank Keith Stolworthy for the help he has given during this entire process, and Peter Halverson, Marina Samuels and Eric Dodgen for the help in testing and data analysis. I gratefully acknowledge the assistance of Kevin Cole of the Department of Mechanical Engineering for help in the test setup and Dr. Eggett of the Department of Statistics for his consultation on the statistical analysis. I also gratefully acknowledge Crocker Spinal Technologies, Inc., the Department of Mechanical Engineering, and the BYU Technology Transfer Office for funding this work.

Finally, I would be remiss if I did not acknowledge the impact of good people in my life: my parents whose encouragement and support have shaped who I am; friends and family who continue to believe in me and my dreams; teachers and professors from grade school to university who saw potential in me and helped to develop it; my exceptional advisor who continued the legacy of my parents and never set limits on my achievement; and Heavenly Father, without whom this would be meaningless.

TABLE OF CONTENTS

LIST OF TABLES

LIST OF FIGURES

NOMENCLATURE

FSU	Functional spinal unit
IVD	Intervertebral disc
AR	Axial rotation
FE	Flexion-extension
LB	Lateral bending
K_{NZ}	Stiffness in the neutral zone
ROM	Range of motion
NZ	Neutral zone
NZR	Neutral zone ratio

CHAPTER 1. INTRODUCTION*

The primary objective of this research is to evaluate the effects of degeneration on the torque-rotation response of the lumbar functional spinal unit (FSU) under a compressive follower load. This thesis adds to previous work by conducting the tests under physiologic conditions (at body temperature and a compressive follower load), and by analyzing the effect of degeneration on range of motion (ROM), stiffness, hysteresis area, and normalized hysteresis. Because no mathematical model exists for lumbar spine segmental rotations, a portion of this thesis evaluates potential methods for curve fitting the torque-rotation curves. The Dual Inflection Point (DIP) Boltzmann equation was developed during the course of this research and is presented here as a method for fitting spinal motion data wherein a physical meaning can be assigned to each of the model coefficients. By using the DIP-Boltzmann curve, we can easily calculate all of the parameters of interest.

Spinal disc degeneration is a process that occurs naturally as an individual ages or as a result of degenerative disc disease. It has been shown that increased joint laxity is a symptom of disc aging and degeneration [2, 3]. It has also been proposed that disc degeneration is accelerated by abnormal loading conditions, such as overloading or immobilization [4–6]. Methods for testing and interpreting spinal biomechanical data continue to improve, giving more insight into the causes and effects of degeneration in the lumbar spine. Better understanding of the mechanical response of the FSU of the lumbar spine not only improves current treatment approaches, but also provides functional specification data that facilitates the design of improved spinal implants.

1.1 Document Organization

The remainder of this chapter provides a discussion on several key aspects of spine segment testing that are relevant for the work represented by this thesis. It also contains a literature review

*Portions of this chapter are currently in review for publication in [1] or are being prepared for submission to *The Spine Journal* or a similar venue.

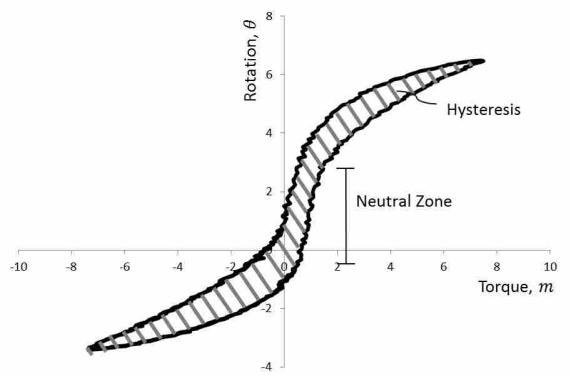

Figure 1.1: The torque-rotation curve for lumbar spinal segments in flexion-extension (FE) and lateral bending (LB) has a sigmoidal shape with characteristic hysteresis and a neutral zone.

of similar work published previous to this thesis. Chapter 2 contains an evaluation of four potential models for the lumbar segmental torque-rotation curve and presents the Dual Inflection Point (DIP) Boltzmann as a candidate solution. Chapter 3 presents the testing conducted on 21 FSUs and analyzes the effect of degeneration, segment level, temperature, and follower load on stiffness, range of motion, hysteresis area, and normalized hysteresis. Chapter 4 contains a summary of the work presented in this thesis and recommendations for future work.

1.2 Testing of the Intervertebral Disc

The motion of the lumbar spine is typically characterized in three modes of loading: flexion-extension (FE), lateral bending (LB), and axial rotation (AR). The resulting torque-rotation curve is distinctly sigmoidal (S-shaped) in FE and LB, but often has a more linear response in AR.

A typical torque-rotation curve is illustrated in Figure 1.1. In spinal biomechanics, the convention is to plot the torque on the horizontal axis and the rotation on the vertical axis. The sigmoidal response is characterized by a predictable hysteresis, attributable to the viscoelastic property of biological tissues [7–9]. Another characteristic typical of spinal motion is the linear midrange portion of the curve, often called the neutral zone. In this region, the intervertebral disc undergoes a large rotation with little change in torque [10, 11].

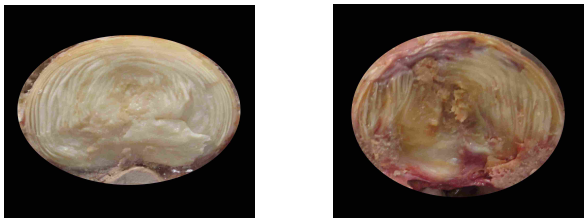

(a) (b)

Figure 1.2: Comparison of a grade I (healthy) disc (a) and a grade V (degenerated) disc (b). Note the difference in color and fiber structure. The degenerated disc also has several indications of vascularization, tearing, and other pathological damage to the annulus fibrosus.

1.3 Degeneration of the IVD

The intervertebral disc consists of the annulus fibrosus (a ring of fibrocartilage) surrounding the nucleus pulposus (a jelly-like center). The annulus fibrosus provides support, while the primary function of the nucleus pulposus is to absorb impact [9]. As the disc ages, it loses water content and height [12]. With increasing degeneration, the annulus fibrosus begins to break down and clefts begin to appear in the disc. Other histologic changes occur as well, including ingrowth of nerves and blood vessels, sclerosis, calcification of the endplates which connect the disc to the vertebral bodies, and osteophyte formation [13]. Figure 1.2 compares the macroscopic changes between a healthy and a degenerated disc. While there is some debate as to the precise definition of degeneration, we will assume any compositional changes that result in a weakened disc are associated with a degenerated disc. Adams and Roughley provide a discussion on the definition of degeneration [6].

1.4 Physiologic Testing Conditions

Previous studies on the biomechanical response of the lumbar FSU had similar objectives to the current research, but their testing was performed without a follower load and at room temperature. The importance of testing with a follower load has been researched by several groups over the last decade [14–18]. Spinal muscles can induce a compressive follower load in the lumbar spine [19]. Although the testing is performed on fresh-frozen cadaver spines, we want to simulate as far as possible the physiologic conditions of the lumbar spine. By testing at body temperature, with a compressive follower load, we expect to obtain more physiologically relevant results.

1.5 Degeneration Grading Scales

In this study we used the Thompson scale to identify the grade of degeneration [20, 21]. The Thompson scale is a macroscopic grading that ranks intervertebral disc degeneration from I to V based on the morphological characteristics of the disc and facets.

Several studies have shown the correlation between magnetic resonance imaging (MRI) and macroscopic grading using the Thompson scale [22, 23]. This can be advantageous for application to patients experiencing lower back pain; the grade of degeneration of the targeted disc, measured by MRI, could influence the method of treatment or prescribe a stabilization device with a tailored stiffness.

1.6 Literature Review

The research that has been done to date has addressed the problem in different ways. Krismer *et al.* sought to determine the degree to which disc degeneration affects axial rotation of the lumbar functional spinal unit [24]. The study included 36 FSUs, ages 20 to 92 years. The loading was applied in discrete steps. The results showed that range of motion (ROM) in axial rotation increased with degeneration.

Mimura *et al.* measured the change in ROM, neutral zone (NZ), and the ratio of NZ to ROM (NZR). The study included 47 discs, ages 35 to 64 years. The researchers were specifically looking at the relationship between spinal instability and disc degeneration. They reported no significant change in ROM and NZ due to degeneration in FE. In LB, they reported a statistically significant decrease in ROM but no significant change in NZ. In AR, they reported an increase in ROM, but it was not statistically significant. [3]

Tanaka *et al.* also conducted a similar study [23] in which the moments were simulated by applying dead weights to the functional spinal units (FSUs) in six steps (i.e., stepwise instead of continuous loading). They reported an increase in flexibility in the upper lumbar spine (T12-L4) in FE and AR up to grade IV degeneration and an increase in flexibility in the lower lumbar spine (L4-S1) in AR and LB at grade III.

Quack *et al.* used an *in vivo* mobility test called the modified Schober to measure mobility of 112 female subjects with lower back pain [25]. The mobility was correlated with degenera-

tion, as determined by magnetic resonance imaging. They did not find a statistically significant correlation between the modified Schober test and MRI findings.

Fujiwara *et al.* found that there are motion differences, primarily attributed to morphologic differences in vertebral bodies, between the two sexes [26]. Nachemson *et al.* also found a difference in mechanical behavior of discs for male vs. female, but again attributed the difference to cross-sectional area (CSA) rather than intrinsic properties [27]. The difference in CSA was accounted for in this research.

Yamamoto *et al.* reported that intervertebral level can have an effect on flexibility [28]. Laud *et al.* tested the hypothesis that the human lumbosacral joint (L5-S1) behaves differently from L1-L5 joints [29]. The results showed a statistically significant difference in FE but not in LB. Tanaka *et al.* also reported a difference in kinematic properties between upper lumbar and lower lumbar, but they grouped L4-L5 with L5-S1 [23]. For this research, we chose to group L4-L5 with L3-L4, based on the results from Laud in 2007 and based on visual inspection of the data collected: the L4-L5 segments performed similarly to the L3-L4 results in stiffness and range of motion.

CHAPTER 2. DIP-BOLTZMANN SIGMOID CURVE FIT*

2.1 Introduction

The objective of this chapter is to provide a mathematical description of the complete torque-rotation curve of the lumbar spine functional spinal unit (FSU) such that the model parameters have physical meaning. Such a model can tell us more about the effects of degeneration, testing conditions, and other factors that are expressed in the change in spinal motion [30]. No such modeling technique currently exists. Improved understanding of the motion of the spine will also facilitate the design of improved spinal implants. Design of future implants can be based on functional specifications derived from the DIP-Boltzmann parameters.

A strong motivation for developing a standard curve fit for spinal motion is to enable the comparison of data across studies. It can be applied to previous studies, increasing their contribution. This model can be used to predict spinal motion and can be used as a tool for designing spinal devices that better approximate the natural motion of the spine. The Boltzmann sigmoid was chosen as the basis for the curve fit; it was modified to better describe the lumbar spinal motion. By ensuring physical meaning of the parameters of the Dual Inflection Point (DIP) Boltzmann sigmoid, the contribution of this curve fit is increased, as it inherently describes the range of motion, hysteresis, and midrange (or neutral zone) stiffness.

2.2 Background

The motion of the lumbar spine is typically characterized in three modes of loading: flexion-extension (FE), lateral bending (LB), and axial rotation (AR). The resulting torque-rotation curve is distinctly sigmoidal (S-shaped) in FE and LB, but often has a more linear response in AR.

*Portions of this chapter are currently in review for publication in [1].

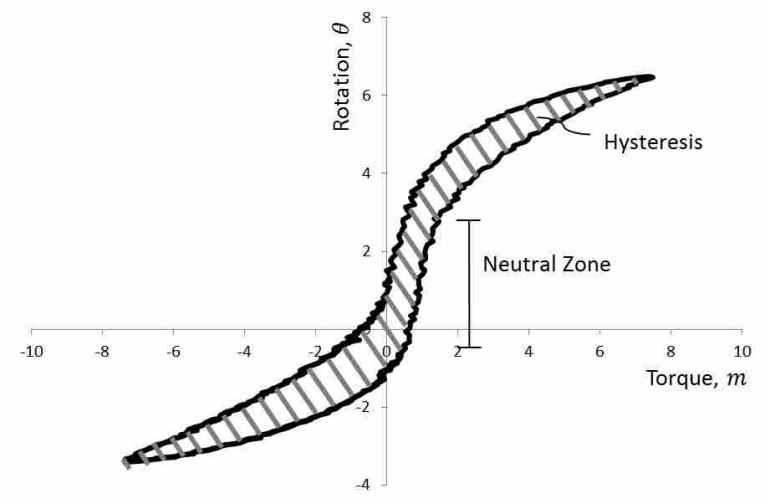

Figure 2.1: The torque-rotation curve for flexion-extension (FE) and lateral bending (LB) has a sigmoidal shape with characteristic hysteresis and a neutral zone.

A typical torque-rotation curve is illustrated in Figure 2.1. In spinal biomechanics, the convention is to plot the torque on the horizontal axis and the rotation on the vertical axis. The sigmoidal response is characterized by a predictable hysteresis, attributable to the viscoelastic property of biological tissues [7–9]. Another characteristic typical of spinal motion is the linear, midrange portion of the curve, often called the neutral zone. In this region, the FSU undergoes a large rotation with little change in torque [10, 11].

The current state of the practice for describing the motion of the lumbar spine is to report the range of motion and the midrange, or neutral zone, stiffness. The objective of this work is to present a regression model that will capture more information about the torque-rotation curve of the lumbar spine (e.g., hysteresis and the points where the stiffness changes). While it is important to model more of the behavior, it is also important to maintain simplicity of the model and significance of the model parameters.

2.2.1 Physical Testing

The data used in this paper were obtained from testing conducted on 21 functional spinal units (FSU) from 8 cadaveric lumbar spines. The spines were obtained from an accredited tissue bank following an approved Institutional Review Board (IRB) acquisition protocol. They were

wrapped in saline-soaked sterile mats to prevent dehydration and stored at -20 °C. Freeze/thaw cycles were minimized [31].

The lumbar spines were prepared according to the following protocol:

- All excess muscle and fat tissue was removed;
- The spine was separated into FSUs, from L1-L2 to L5-S1;
- The vertebral bodies of each FSU were potted in Bondo auto body filler to provide a gripping surface;
- The FSUs were secured in the testing apparatus;
- A 440 N compressive follower load was applied during testing.

A more complete description of specimen preparation and test setup is included in Chapter 3.

The testing was done on the custom spine tester built by the BYU Applied Biomechanical Engineering Laboratory (BABEL) that was largely based on the design published by Oxland *et al.* [32]. It was modified to include a guided follower load, a multi-camera three-dimensional motion tracking system, and an environmental chamber that is capable of maintaining the environment at desired settings of temperature and humidity. The control system of the simulator used a torque-sensor and rotary-encoder to control a stepper motor.

The FSUs were tested in all three modes of loading at both body and room temperature in a near 100% humidity environment [33–35]. A compressive follower load of 440 N was applied to simulate physiologic conditions [15, 36]. A design of experiments was used to vary the order of the tests.

The FSUs were all tested at a continuous rate of loading of 1°/sec to a maximum torque response of ±7.5 N·m [37]. The torque and position data were recorded through a Labview program. Three-dimensional position data was obtained after testing by using optical marker tracking. The image capture rate was synchronized with the recording rate of the control system.

The motion in the lumbar spine consists of both rotations and translations. We measured the rotations of the vertebral bodies in the direction of the applied moments to isolate the torque response of the segment in the primary modes of loading [3, 38, 39].

2.2.2 Regression Models

To find the best approach for fitting the torque-rotation curve of the lumbar spine, several other approaches were explored. The benefits and limitations of each are outlined here. A comparison is also made between the number of independent parameters required by each model to define the curve. The more parameters there are, the more complicated the model. However, too few parameters limits the data retained in the model.

2.2.2.1 Range of Motion and Neutral Zone Approach

A commonly used approach for describing the motion of the lumbar spine is to define the range of motion of the segment [17,24,26,38–41]. Some researchers have also identified the neutral zone in their results [3]. The curve definition using these two factors is illustrated in Figure 2.2.

This model is simple to implement and describes two key aspects of the torque-rotation curve, i.e., range of motion and neutral zone stiffness. It requires only two parameters to define the range of motion, and four parameters if the neutral zone is included. Range of motion is the easiest to measure and is the most frequently reported feature of the torque-rotation response. By only reporting range of motion and neutral zone stiffness, however, we limit the amount of information retained in the model. For example, hysteresis and points of inflection where the stiffness changes are not reported.

2.2.2.2 Exponential Fit

As we researched possible curve fits for the spinal rotations, an exponential fit was presented as a reasonable approximation:

$$\theta = C e^{\alpha m} + B \tag{2.1}$$

For a smooth sigmoidal response, this curve has a very good fit as measured by the coefficient of determination, R^2 (see Figure 2.3). However, the motion of the FSU is often mathematically imperfect; the exponential fit does not correspond exactly to these erratic curves. Also, to fit the torque-rotation curve, the data must be parsed into four separate curves because the exponential fit

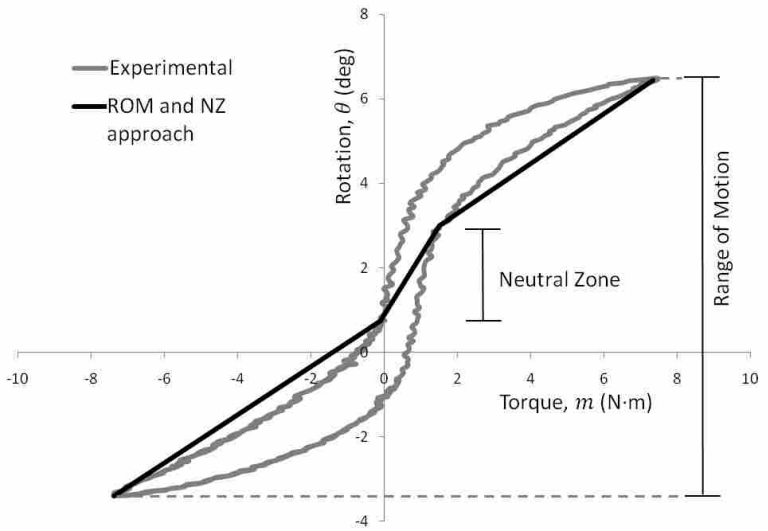

Figure 2.2: A common approach for describing spinal rotations is to define the range of motion of the spinal segment and its stiffness in the neutral zone.

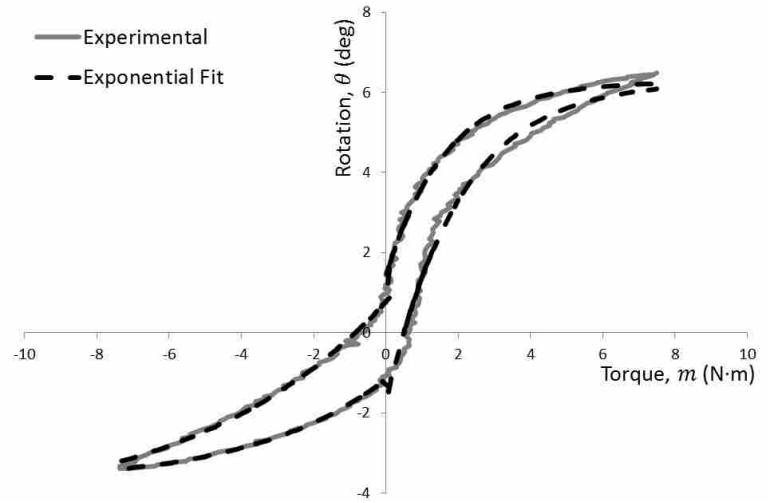

Figure 2.3: The exponential fit, $\theta = Ce^{\alpha m} + B$, has a high R^2 value for well-behaved curves but has a lower R^2 for erratic curves. It requires four instances of the curve fit to fully describe the motion.

does not allow the torque to change sign. Therefore, a total of twelve independent parameters are needed to define each torque-rotation response.

2.2.2.3 Boltzmann Sigmoid Fit

The Boltzmann sigmoid, shown in Figure 2.4, is presented here as a possible method for fitting the torque-rotation curve of the lumbar spine. Because of its applicability to dose-response systems and muscle activation response, the Boltzmann sigmoid is often used in these biological applications, although it is not always directly cited [42–46]. It has also been used in chemorheology [47, 48] and other applications [49]. Its use in describing lumbar spinal motion has not yet been reported.

For fitting a large number of curves, the Boltzmann sigmoid is initially preferable to the exponential fit because the experimental results can be described by two curves (upper and lower) instead of four. This also reduces the number of independent parameters needed to describe the curve to eight. The equation for this curve fit is:

$$\theta = \frac{A-B}{1+e^{\alpha(m-m_0)}} + B \tag{2.2}$$

By using an upper and lower curve, the hysteresis attributable to the viscoelastic behavior of the intervertebral disc is preserved. It is possible to create a single curve that averages the loading and unloading of the disc, but this would limit the information contained in the curve fit. The original Boltzmann sigmoid curve, like the exponential fit, lacks robustness for erratic curves. It also fails to accurately define the midrange, or neutral zone, stiffness.

2.3 Model Description

The proposed Dual Inflection Point (DIP) Boltzmann, shown in Figure 2.5, has a coefficient of determination comparable to that of the exponential curve fit and can fit the full torque-rotation response with two curves (upper and lower). The unmodified Boltzmann sigmoid defines symmetric behavior, but spinal motion is asymmetric, especially in flexion-extension. The model was modified to capture this asymmetry in the equation by introducing a second inflection point:

$$\theta = \frac{A}{1+e^{\alpha_1(m-m_1)}} - \frac{B}{1+e^{\alpha_2(m-m_2)}} + B \tag{2.3}$$

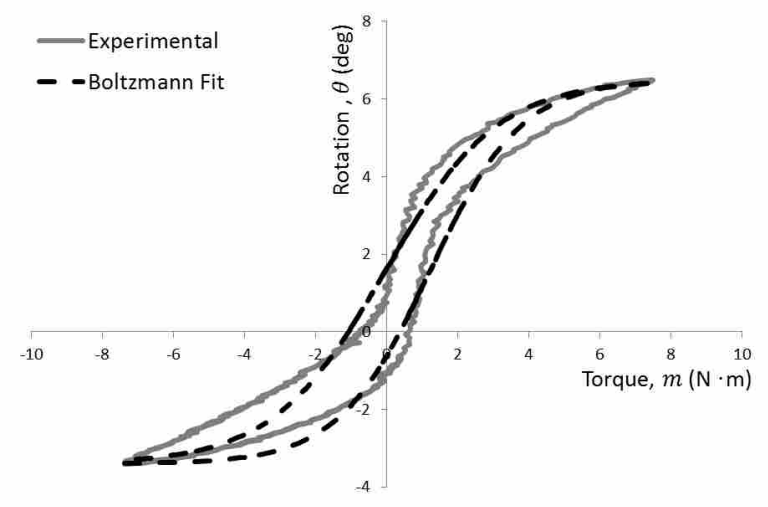

Figure 2.4: The Boltzmann sigmoid, $\theta = \frac{A-B}{1+e^{\alpha(m-m_0)}} + B$, approximates the sigmoidal shape of the motion of the spine, but does not accurately capture the midrange, or neutral zone, stiffness.

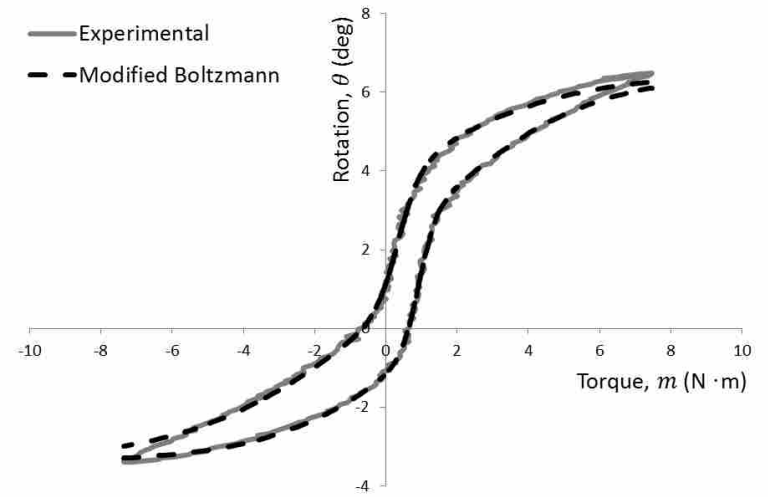

Figure 2.5: The DIP-Boltzmann, $\theta = \frac{A}{1+e^{\alpha_1(m-m_1)}} - \frac{B}{1+e^{\alpha_2(m-m_2)}} + B$, has a comparable R^2 value to that of the exponential fit and requires half the number of curves to fully describe the motion of the lumbar spine.

If the model is unconstrained, twelve parameters are required to define the full torque-rotation response of the lumbar spine. However, one of the key features of this model is that each of the parameters of the DIP-Boltzmann curve can each be described physically (refer to Figure 2.6). The variable A represents the minimum rotation of the spinal segment and B represents its maximum rotation. Together, $B-A$ defines the segment's range of motion. The variables m_1

and m_2 are the points of inflection of the curve and they identify the boundaries of the neutral zone. Finally, α_1 and α_2 are associated with the rates of change of the curve at m_1 and m_2, respectively. Since A and B are the same for both curves, a total of ten independent parameters describe the entire response, including hysteresis.

This curve fit can be applied to rotations recorded in degrees or radians; the difference in the curve fit is only in the units conversion of A and B. To apply the DIP-Boltzmann sigmoid, the data is parsed into two curves: from minimum to maximum torque (the lower curve) and from maximum to minimum torque (the upper curve).

Depending on the goal of the study, the torque-rotation curves can be centered vertically at zero. A vertical shift maintains the same range of motion, $B-A$, and does not alter any of the other properties of the torque-rotation curve, but it does facilitate comparison between curves.

The DIP-Boltzmann equation is fit to the upper and lower curves by minimizing the sum of squared errors between the curve fit and the actual rotations. With this fit, the curve is over defined, so there are a number of possible solutions. The best description of the curve is where the points of inflection, m_1 and m_2, occur on either end of the neutral zone. These points can be defined by the user and constrained in the model. Ultimately, we chose to constrain the endpoints, A and B, rather than the inflection points. This method ensures that the endpoints are the same for both the upper and lower curves.

With the DIP-Boltzmann sigmoid fit, the hysteresis can be quantified by subtracting the integrals of the upper and lower curves to calculate the difference in area. The integral of the DIP-Boltzmann sigmoid from minimum to maximum torque is:

$$\begin{aligned}\int_{m_{min}}^{m_{max}} \theta \, \mathrm{d}m = A\left(m_{max}-m_{min}\right) - \frac{A}{\alpha_1}\ln\left[\frac{1+e^{\alpha_1(m_{max}-m_1)}}{1+e^{\alpha_1(m_{min}-m_1)}}\right] \\ +\frac{B}{\alpha_2}\ln\left[\frac{1+e^{\alpha_2(m_{max}-m_2)}}{1+e^{\alpha_2(m_{min}-m_2)}}\right]\end{aligned} \tag{2.4}$$

The hysteresis area is the difference in the intergral evaluated for the upper curve and the integral evaluated for the lower curve.

The midrange or neutral zone stiffness can also be obtained mathematically from the DIP-Boltzmann model by calculating the rotations at the inflection points, or θ_1 and θ_2 at m_1 and m_2.

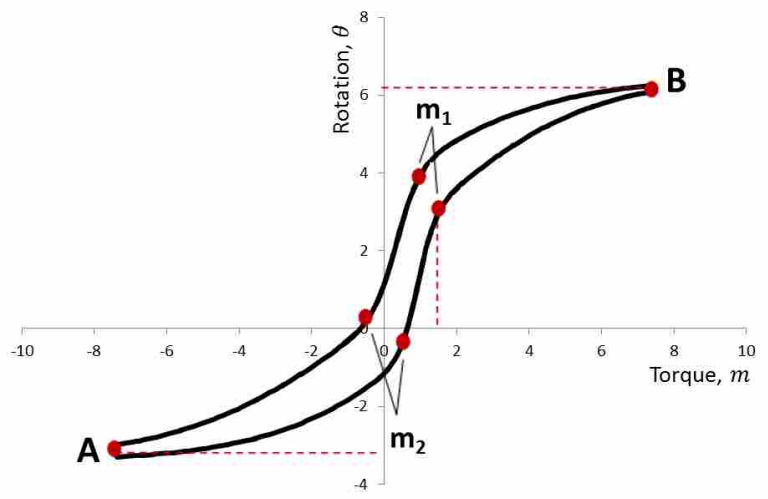

Figure 2.6: A physical meaning can be assigned to each of the coefficients of the DIP-Boltzmann model: A and B are the minimum and maximum deflections, respectively; m_1 and m_2 identify the points where the curve changes stiffness; and α_1 and α_2 are associated with the rates of change of the curve at m_1 and m_2, respectively.

The neutral zone stiffness, K_{NZ}, is the ratio of these differences:

$$K_{NZ} = \frac{m_2 - m_1}{\theta_2 - \theta_1} \tag{2.5}$$

This stiffness represents the inverse of the slope of the line in the neutral zone.

2.4 Model Results

Sixty-three torque-rotation curves obtained from our testing were fit with the linear, Boltzmann sigmoid, exponential, and DIP-Boltzmann sigmoid curves. The goodness of fit was measured by the coefficient of determination, R^2. Table 2.1 shows a comparison of these four methods for the twenty-one segments in all three modes of loading. The linear fit has the lowest coefficient of determination, with an average R^2 value of 0.8044. The Boltzmann sigmoid has an average R^2 value of 0.9934. The exponential and DIP-Boltzmann curve fits have almost the same average R^2 value: 0.9960 and 0.9961, respectively.

When we considered each mode of loading separately, the DIP-Boltzmann had a higher average coefficient of determination in both axial rotation and lateral bending, while the exponential curve had a better fit in flexion-extension. We conclude that goodness of fit of the exponential

and DIP-Boltzmann curves are comparable, but the DIP-Boltzmann curve has the added benefit of having physical meaning for all parameters.

The R^2 values reported in Table 2.1 were all obtained without constraining any of the curve parameters. The average R^2 value for the DIP-Boltzmann curve when A and B are constrained to be the endpoints of the curve is 0.9941.

The stiffness was calculated for each of these curves using the DIP-Boltzmann and compared to the slope of the midrange or neutral zone. An analysis of variance comparing the two methods showed that there was no statistical difference between the two ($p = 0.9916$). The coefficient of determination was 0.9425. This suggests that the DIP-Boltzmann can be used to calculate the stiffness of the torque-rotation curve.

2.5 Discussion and Conclusions

Data from spine testing have generally been reported as range of motion and neutral zone stiffness rather than the full sigmoid shape. These are the most descriptive parameters of the curve, but they do not fully define the motion of the lumbar spine: they do not describe the hysteresis, nor do they identify the change in stiffness from the neutral zone to the end of the curve.

The Dual Inflection Point (DIP) Boltzmann is presented as a way to concisely represent the full motion of the lumbar spine. The curve fit parameters have physical meaning (e.g., range of motion and boundaries of neutral zone), and other important characteristics (e.g., stiffness of neutral zone and hysteresis) can be directly calculated from them. While an average of the upper and lower curves could also be found using the DIP-Boltzmann curve, it is not recommended, as valuable information (e.g., hysteresis) is lost.

Table 2.1: Comparison of R^2 values for four different fits applied to 63 torque-rotation curves. The average R^2 value is reported, along with the highest and lowest R^2 values for the 63 curves.

Method	Average R^2	Highest R^2	Lowest R^2
Linear	0.8044	0.9854	0.4277
Boltzmann sigmoid	0.9934	0.9997	0.9583
Exponential	0.9960	0.9997	0.9656
DIP-Boltzmann	0.9961	0.9998	0.9638

The number of parameters required for the DIP-Boltzmann in the unconstrained case is twelve. When A and B are constrained to be the minimum and maximum rotations of the curve, respectively, the number of independent parameters required is reduced to ten. For the exponential fit, the number of independent parameters is also twelve in the unconstrained case. If constraints are applied, this could potentially be reduced to ten: the variable, B, could be constrained to be the maximum rotation for each instance of the curve fit (representing one-fourth of the full torque-rotation curve). The original Boltzmann sigmoid fit requires eight independent parameters for the unconstrained case, or six independent parameters if A and B are constrained to be the limits of rotation. The ROM approach only requires two parameters, A and B; adding the neutral zone stiffness increases the number of parameters to four.

Having a standard curve fit means we can compare data across studies. This is especially beneficial when considering the high costs of cadaveric testing. The parameters of the model will also provide input to the development process of creating devices with the same motion response as that exhibited by the spine.

For consistency, we recommend that the DIP-Boltzmann be used to characterize all three modes of loading, even though axial rotation exhibits a much more linear profile than flexion-extensions and lateral bending. By doing so, the method of evaluating the curve parameters will be consistent for all three modes of loading.

Because we chose to constrain A and B and allowed m_1 and m_2 to be set by the model, the neutral zone was not always clearly demarcated. When applying the curve fit, we recommend that the inflection points be compared to m_1 and m_2 before the neutral zone stiffness is calculated.

CHAPTER 3. MECHANICAL RESPONSE TESTING*

3.1 Introduction

Spinal disc degeneration is a process that occurs naturally as an individual ages or as a result of degenerative disc disease. It has been shown that increased joint laxity is a symptom of disc aging and degeneration [2, 3]. It has also been proposed that disc degeneration is accelerated by abnormal loading conditions, such as overloading or immobilization [4–6]. Methods for testing and interpreting spinal biomechanical data continue to improve, giving more insight into the causes and effects of degeneration in the lumbar spine. Better understanding of the mechanical response of the functional spinal unit (FSU) of the lumbar spine not only improves current treatment approaches, but also provides functional specification data that facilitates the design of improved spinal implants.

Although torque-rotation behavior of degenerated spinal segments has previously been published, these studies were performed at room temperature without the presence of a follower load. These studies found correlations between disc degeneration and segmental flexibility for some modes of loading, but the results often lacked statistical significance. The objective of this research was to show the effects of degeneration on the torque-rotation response of the FSU under a compressive follower load. We also evaluated the effects of temperature and follower load on four key parameters: segmental stiffness, range of motion, hysteresis area, and normalized hysteresis. The grade of degeneration was measured using the Thompson scale [20].

Previous studies of a similar nature have only examined the rotations of the FSU, including the full range of motion (ROM) and the range of the neutral zone [3, 23, 24]. Although midrange (or neutral zone) stiffness has been reported in some lumbar spine segmental testing [35], it has not been reported in any of these related studies. Range of motion is included in the present work, as well as the stiffness in the midrange. Parameters included here that have not been typically reported

*Portions of this chapter will be submitted for publication in *The Spine Journal* or a similar venue.

in lumbar spine segmental testing are the hysteresis area and normalized hysteresis (hysteresis area/ROM). By using the DIP-Boltzmann curve (refer to Chapter 2), we can easily calculate all of these parameters. This curve and the additional parameters capture more information about the quality of motion [30] and the changes in mechanical response associated with degeneration.

3.1.1 Motivation

There is no consistent relation between mechanical response of the spine and the level of degeneration. To design spinal implants, it is necessary to know what motion is desired. By correlating the torque-rotation response with the level of degeneration, devices can be designed to an appropriate range of motion and stiffness, potentially reducing the impact on adjacent discs [4]. The prevalence of lower back pain is another key motivation for this work. Eleven percent of Americans have an episode of severe back pain each year [50] and back pain accounts for 1 million missed work days annually in the United States [51]. Disc degeneration is associated with lower back pain [52]; therefore, understanding the biomechanics associated with disc degeneration will enable better treatment methods for lower back pain.

Part of the motivation for doing this testing is that test methods have changed (and presumably improved) in the last decade; it may be possible to find statistical significance where previous studies had only been able to identify trends. Also, new methods for interpreting the data allow us to more easily investigate the changes in stiffness and hysteresis.

3.2 Methods and Materials

Testing was conducted on 8 cadaveric lumbar spines, ages 46 to 100 years, with no known spinal disorders. The spines were separated into 21 single-level FSU testing specimens: 6 from L1-L2, 1 from L2-L3, 6 from L3-L4, 2 from L4-L5, and 6 from L5-S1. Because of the small sample size, the L2-L3 segment was grouped with L1-L2 for statistical testing and the L4-L5 segments were grouped with L3-L4 [29]. (A second L2-L3 segment failed in testing and was excluded from the population.) The spines were obtained from an accredited tissue bank following an approved Institutional Review Board (IRB) acquisition protocol. They were wrapped in saline-soaked sterile mats to prevent dehydration and stored at -20 °C. Freeze/thaw cycles were minimized [31].

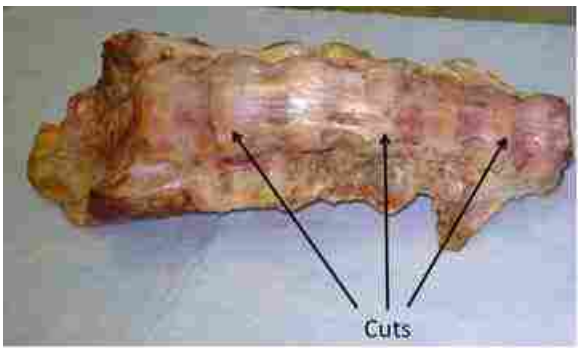

Figure 3.1: The FSUs were separated by cutting through every other intervertebral disc, as indicated.

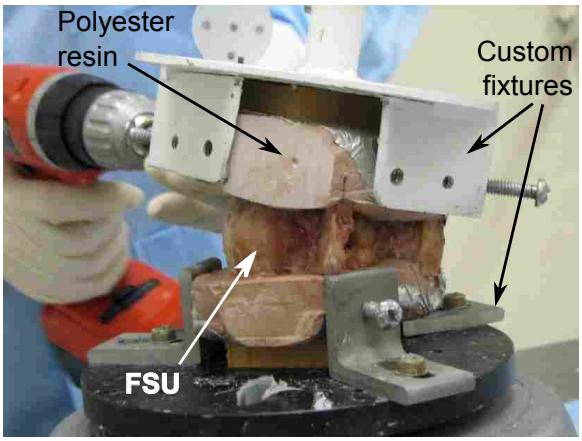

Figure 3.2: The FSU was secured in custom fixtures with screws and polyester resin.

3.2.1 Specimen Preparation

With the lumbar spine thawed, the FSUs were separated by cutting through every other intervertebral disc (see Figure 3.1); e.g., for the L1-S1 lumbar spine, the spine was cut at the T12-L1 disc, the L2-L3 disc, and the L4-L5 disc.

Excess muscle and adipose tissue was removed to expose the ligaments and bone. The distal half of the vertebral bodies were prepared for potting by scraping away the soft tissue and blotting with a paper towel. A two-part polyester resin (Bondo auto body filler) was used to adhere to the vertebral body and provide a larger gripping surface. After the two bodies were potted, they were each secured in custom fixtures and several drywall screws were driven through the resin to the vertebral body to anchor it firmly (see Figure 3.2).

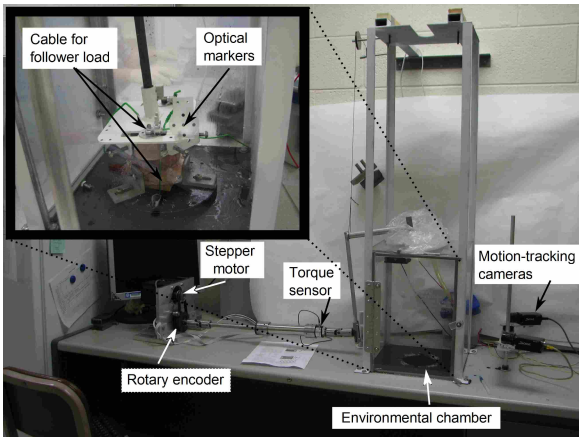

Figure 3.3: Testing was done on a custom spine tester. A stepper motor was used to control rotation. Motion-tracking cameras were used to obtain rotations.

The FSU was positioned so that the posterior third was aligned with the follower load path [15]. The upper potting fixtures were aligned so the follower load acted through the approximate axis of rotation of the FSU. Optical markers were attached to the upper potting fixture to track the rotations of the FSU. It was assumed that the vertebral bodies were rigidly secured in the fixtures. The FSU was secured in the testing apparatus and a 440 N compressive follower load was attached by cable wire to the upper potting fixture.

3.2.2 Physical Testing

The testing was done on a custom spine tester built by the BYU Applied Biomechanics Engineering Laboratory (BABEL) that was largely based on the design published by Oxland *et al.* [32]. It was modified to include a guided follower load, a multi-camera three-dimensional motion tracking system, and an environmental chamber that is capable of maintaining the environment at desired settings of temperature and humidity. The control system of the simulator used a torque-sensor and rotary-encoder to control a stepper motor.

The FSUs were tested in all three modes of loading at a continuous rate of loading of $1^\circ/\text{sec}$ to a maximum torque response of ±7.5 N·m [37]. Testing was conducted at both body temperature (39 ± 2 °C) and room temperature (21 ± 1 °C) in a near 100% humidity environment [33–35]. A compressive follower load of 440 N was applied to simulate physiologic conditions [15, 36]. Data was also collected on a subset of the 21 FSUs (15 FSUs) for all three modes of loading and at both

temperatures without the follower load to compare the effects of the load. The torque and position data were recorded through a Labview program. Three-dimensional position data was obtained after testing by using optical marker tracking. The image capture rate was synchronized with the recording rate of the control system.

Testing was done in random order, using a design of experiments. All tests on a given segment were completed in a single testing session. Temperature was treated as a block variable, while loading direction and application of follower load were allowed to vary.

Because we were conducting tests at two different temperatures, we determined the rate of heat transfer in the intervertebral disc using a thermocouple inserted into the center of a T12-L1 disc. It took 20 minutes to reach 38°C from 21.5°C and 43 minutes to cool down from 40°C to 21.5°C. Based on this test, we allowed a minimum of 1 hour between tests conducted at different temperatures. During this time, the segment was wrapped in a saline-soaked sterile mat to maintain hydration.

A hot and a cold humidifier were used to regulate temperature and humidity inside the environmental chamber. Although the chamber was kept at $> 95\%$ humidity, the discs were sprayed regularly with phosphate buffered saline to ensure adequate moisture and salinity levels.

Two cameras were placed at angles to each other to provide 3-D rotational data. The cameras (Basler Vision) viewed the disc through a glass plate; the plate was kept free from condensation by applying a clear, viscous gel (JAWS Spit Antifog) to the inside of the glass and by heating the glass externally. Camera calibration was performed within the chamber to account for optical aberration from the environmental chamber.

The segments were preconditioned for 30 cycles before the first test on each segment, and for a minimum of 10 cycles before subsequent tests (until a repeatable behavior was exhibited). We started each cycle of testing from the FSU's neutral position; i.e., under the applied follower load, the rotation was calibrated to zero at zero torque. The motivation for this was to ensure the line of action of the follower load passed through the axis of rotation of the disc so that it would not contribute an additional moment to the system. It is noted that the axis of rotation of the FSU translates during rotation [53, 54].

A pure moment load was applied using a stepper motor with 0.09° resolution. To test in lateral bending, the segment was rotated 90°. To test in axial rotation, the motor was moved to the top of the apparatus (refer to Figure 3.3).

The motion in the lumbar spine consists of both rotations and translations. We measured the rotations of the vertebral bodies in the direction of the applied moments to isolate the torque response of the segment in the primary modes of loading [3, 38, 39].

3.2.3 Macroscopic Grading

After the mechanical testing was completed, the grade of degeneration was evaluated by the Thompson scale [20]. The Thompson scale is a macroscopic grading that ranks intervertebral discs from I (no degeneration) to V (advanced degeneration), based on the morphologic characteristics of the disc and facets. The purpose of this study is not to investigate correlation between grading systems, so only the Thompson scale was used. It was modified to allow a transverse cross-section cut, exposing the disc and facets, rather than the prescribed mid-sagittal cut [55].

3.2.4 Data Analysis

The rotations were obtained from the optical motion tracking and the data were prepared for analysis. As part of the research, the results were analyzed for the raw measured torque and for the torque normalized by cross-sectional area (CSA) and by the area moment of inertia. The data were fit with a dual inflection point (DIP) Boltzmann sigmoid curve.

3.2.4.1 Normalized Torque

The difference in cross-sectional area of the IVD, particularly notable between genders, is recognized as a potential cause for differences in torque response [26, 27]. It is common to normalize torque by height, cross-sectional area (CSA), and volume [56–58].

To account for this, and considering the physics of the motion, we chose to normalize torque by both CSA and the area moment of inertia. The moment (or the torque) about a point or axis provides a measure of the tendency of the force to cause a body to rotate about the point or axis [59]. The area moment of inertia is a property of a cross-section that can be used to predict

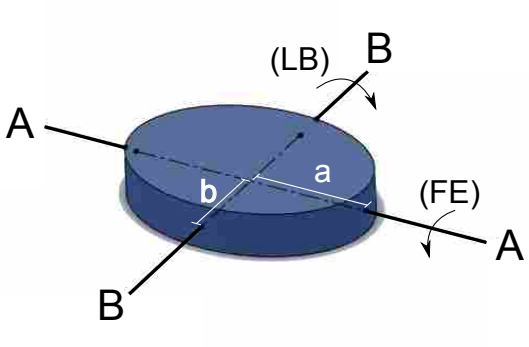

Figure 3.4: The cross-sectional area of the intervertebral disc was approximated as an ellipse, with the semi-major axis of length a and the semi-minor axis of length b. The area moments were taken about the A-A axis for FE and the B-B axis for LB.

the resistance of a body to bending and deflection, around an axis that lies in the cross-sectional plane [60].

For both methods of normalization, the following assumptions were made to simplify the problem. First, the cross-section was approximated as an ellipse with area equal to πab, where a is the length of the semi-major axis and b is the length of the semi-minor axis, as shown in Figure 3.4. Second, the axis of rotation for calculating the area moments was approximated to be the axis passing through the center of the ellipse. Specifically, the area moment for flexion-extension was calculated about the A-A axis and the area moment for lateral bending was calculated about the B-B axis. For axial rotation, the polar moment is the sum of these two area moments. These assumptions make the problem more tractable while maintaining sufficient accuracy to illustrate the effects.

3.2.4.2 DIP-Boltzmann Sigmoid Curve Fit

The change in mechanical response was evaluated based on four parameters: change in ROM, change in stiffness, and change in area hysteresis and normalized hysteresis (area hysteresis/ROM). The current state of the practice for describing the motion of the lumbar spine is to report the range of motion and the midrange, or neutral zone, stiffness. To obtain these and the remaining desired parameters, the raw torque-rotation curves were fitted with a Dual Inflection

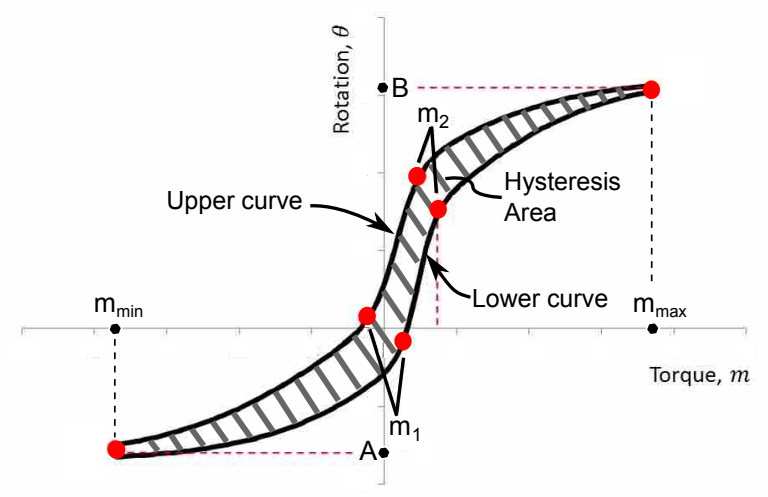

Figure 3.5: A physical meaning can be assigned to each of the coefficients of the DIP-Boltzmann model: A and B are the minimum and maximum deflections, respectively; m_1 and m_2 identify the points where the curve changes stiffness; and α_1 and α_2 are associated with the rates of change of the curve at m_1 and m_2, respectively.

Point (DIP) Boltzmann sigmoid curve. The DIP-Boltzmann equation is

$$\theta = \frac{A}{1+e^{\alpha_1(m-m_1)}} - \frac{B}{1+e^{\alpha_2(m-m_2)}} + B \tag{3.1}$$

where A and B are the minimum and maximum rotations, respectively; m_1 and m_2 identify the inflection points where the curve changes stiffness; and α_1 and α_2 are associated with the rates of change of the curve at m_1 and m_2, respectively.

The torque-rotation curves were centered vertically at zero. A vertical shift maintains the same range of motion, $B-A$, and does not alter any of the other properties of the torque-rotation curve, but it does facilitate comparison between curves.

The DIP-Boltzmann equation was fit to the upper and lower curves by minimizing the sum of squared errors between the curve fit and the actual rotations. We constrained the endpoints, A and B, to ensure the endpoints are the same for both the upper and lower curves. The full set of DIP-Boltzmann model coefficients for the data collected in this study are included in Appendix A.

With the DIP-Boltzmann sigmoid fit, the hysteresis can be quantified by subtracting the integrals of the upper and lower curves to calculate the difference in area. The integral of the DIP-Boltzmann sigmoid from minimum to maximum torque (or from m_{min} to m_{max}, as indicated

in Figure 3.5) is:

$$\int_{m_{min}}^{m_{max}} \theta \, \mathrm{d}m = A\,(m_{max} - m_{min}) - \frac{A}{\alpha_1} \ln\left[\frac{1+e^{\alpha_1(m_{max}-m_1)}}{1+e^{\alpha_1(m_{min}-m_1)}}\right] + \frac{B}{\alpha_2} \ln\left[\frac{1+e^{\alpha_2(m_{max}-m_2)}}{1+e^{\alpha_2(m_{min}-m_2)}}\right] \tag{3.2}$$

The hysteresis area is the difference in the integral evaluated for the upper curve and the integral evaluated for the lower curve. The normalized hysteresis is the ratio of hysteresis area to ROM for the pair of DIP-Boltzmann curves defining the torque-rotation response.

The midrange or neutral zone stiffness can also be obtained mathematically from the DIP-Boltzmann by calculating the rotations at the inflection points, or θ_1 and θ_2 at m_1 and m_2. The neutral zone stiffness, K_{NZ}, is the ratio of these differences:

$$K_{NZ} = \frac{m_2 - m_1}{\theta_2 - \theta_1} \tag{3.3}$$

This stiffness represents the inverse of the slope of the line in the neutral zone.

3.2.5 Statistical Analysis

A statistical analysis was performed to evaluate the significance of the change in the mechanical response due to degeneration. The four parameters associated with the torque-rotation response of the lumbar FSU that are evaluated in this work are:

1. Range of motion, or changes in $A - B$.
2. Midrange stiffness, or changes in K_{NZ}.
3. Hysteresis area, or changes in the difference of the integrals of the upper and lower DIP-Boltzmann sigmoid curves.
4. Normalized hysteresis, or changes in the ratio of hysteresis area to ROM.

The statistical analysis was performed using SAS® 9.2 software. It was set up as a mixed model because segments from the same spine are more likely to be similar than segments from

different spines. The mixed model is a repeated measures analysis of variance. The analysis was performed separately for each loading direction (AR, FE, and LB). The model or fixed effects were temperature, segment, and grade. The LSMeans were calculated for all fixed effects using the Tukey adjustment for multiple comparisons, and the probabilities for all pairwise differences were computed. LSMeans are predicted population margins; that is, they estimate the marginal means over a balanced population. A statistical significance of $\alpha = 0.05$ was used for all statistical tests. A p-value less than 0.05 is considered statistically significant; for this paper, a p-value between 0.05 and 0.07 is considered marginally significant.

3.3 Results

Normalization by CSA or by area moment had very little impact on statistical significance of any of the parameters. Aside from the discussion on the effects of normalization, the results are based on the raw measured torque. Also, aside from comparison between load and no load, the data was evaluated based on the compressive follower load being applied.

Because of challenges with calibrating the location of the follower load with lateral cable pathways, FE data was analyzed only on a portion of the data (on 15 of the 21 segments). Data selection for FE analysis was based on date of testing; as testing progressed, our method of applying the follower load improved so as to reduce the effect of an undesired additional moment from the follower load. The first 6 segments were therefore not included in the analysis for FE loading. This also corresponds to the date when we began testing both with and without a follower load. Statistical results for AR and LB use the full set of data, except when evaluating the effect of the follower load.

Finally, although the stiffness of the upper and lower curves were calculated separately, the statistical results were essentially identical, so upper and lower stiffnesses are generalized as one stiffness in the results.

The means and standard deviations for the four parameters evaluated are listed in Tables 3.1 to 3.4. Table 3.5 gives the means and standard deviations for the DIP-Boltzmann coefficients.

The results from the mixed model are summarized in Table 3.6 for axial rotation, Table 3.7 for flexion-extension, and Table 3.8 for lateral bending. A p-value less than 0.05 is considered

statistically significant; for this paper, a p-value between 0.05 and 0.07 is considered marginally significant. The statistics are described in further detail below.

3.3.1 Effect of Degeneration

The statistical effects for degeneration on stiffness, ROM, hysteresis area and normalized hysteresis are shown in Figure 3.6 for axial rotation, Figure 3.7 for flexion-extension, and Figure 3.8 for lateral bending. For each boxplot, the height of the box represents the interquartile range (the distance between the 25th and the 75th percentiles), the dot in the box interior indicates the mean value, the horizontal line in the box interior indicates the median value, and the vertical lines (or whiskers) extend to the minimum and maximum values of the analysis variable.

Increasing degeneration tended to reduce stiffness from grade I to III and increase stiffness from grade III to V. When considering the LSMeans, or pairwise differences, this effect was statistically significant from grade I to all other grades in AR and from grade V to all other grades in LB.

The effect on ROM was statistically significant in all three modes of loading. Specifically, the increase in ROM was statistically significant in AR from grade I to IV and grade I to V. In FE, the decrease in ROM was statistically significant from grade III to V. In LB, there was a statistically significant decrease in ROM from grade II to grades IV and V.

Hysteresis area generally increased in AR and decreased in LB. In AR, the effect was statistically significant from grades I and II to grades IV and V. In LB, there was a statistically significant decrease in hysteresis area from grade II to V, a marginally significant increase from

Table 3.1: Means and standard deviations for stiffness according to grade of degeneration and listed by direction.

	Stiffness (N·m)		
Grade	AR	FE	LB
I	7.78 ± 3.63	0.24 ± 0.04	1.11 ± 0.67
II	4.27 ± 1.85	0.23 ± 0.06	0.35 ± 0.32
III	4.49 ± 3.08	0.10 ± 0.05	1.03 ± 1.03
IV	2.92 ± 1.70	0.58 ± 0.48	1.47 ± 0.91
V	3.70 ± 2.71	0.98 ± 1.06	4.48 ± 2.82

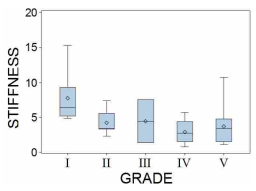

(a) Effect of degeneration on stiffness (N·m) in AR

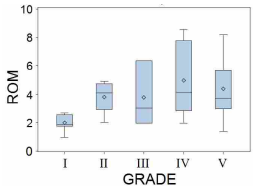

(b) Effect of degeneration on ROM (deg) in AR

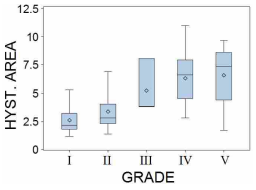

(c) Effect of degeneration on hysteresis area (N·m·deg) in AR

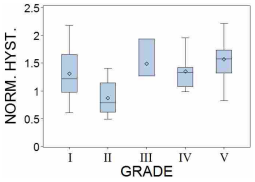

(d) Effect of degeneration on normalized hysteresis (N·m) in AR

Figure 3.6: These boxplots show the effect of degeneration on several parameters in axial rotation.

grade I to II, and a marginally significant decrease from grade II to IV and grade IV to V. There was no statistically significant change in hysteresis area for FE.

Normalized hysteresis is statistically significant for FE, where we see a trend of increasing normalized hysteresis with degeneration. In FE, the effect was statistically significant from grades I and II to grade V, from grade III to grades IV and V, and from grade IV to V. There was no statistical significance for normalized hysteresis in either AR or LB.

Table 3.2: Means and standard deviations for ROM according to grade of degeneration and listed by direction.

	ROM (deg)		
Grade	AR	FE	LB
I	2.00 ± 0.58	11.80 ± 0.55	11.53 ± 6.91
II	3.80 ± 1.18	9.80 ± 1.14	16.30 ± 4.71
III	3.78 ± 2.30	16.45 ± 0.64	11.80 ± 6.07
IV	4.98 ± 2.53	10.83 ± 1.79	9.17 ± 4.03
V	4.40 ± 2.15	9.34 ± 3.98	4.73 ± 3.51

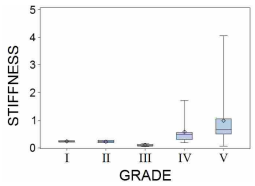

(a) Effect of degeneration on stiffness (N·m) in FE

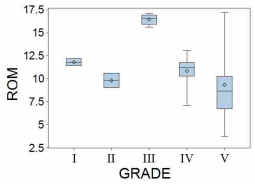

(b) Effect of degeneration on ROM (deg) in FE

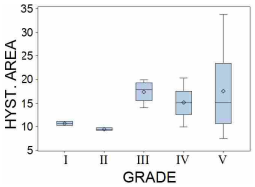

(c) Effect of degeneration on hysteresis area (N·m·deg) in FE

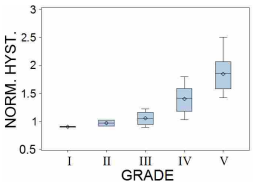

(d) Effect of degeneration on normalized hysteresis (N·m) in FE

Figure 3.7: These boxplots show the effect of degeneration on several parameters in flexion-extension.

3.3.2 Effect of Segment Level

Only three segment levels were considered in the analysis: L1-L2, L3-L4, and L5-S1. The L2-L3 segment was grouped with L1-L2, and the two L4-L5 segments were grouped with L3-L4. The statistical effects of segment level on stiffness, ROM, hysteresis area and normalized hysteresis are shown in Figure 3.9 for axial rotation, Figure 3.10 for flexion-extension, and Figure 3.11 for lateral bending.

Table 3.3: Means and standard deviations for hysteresis area according to grade of degeneration and listed by direction.

	Hysteresis Area (N·m·deg)		
Grade	AR	FE	LB
I	2.58 ± 1.31	10.70 ± 0.58	19.09 ± 5.26
II	3.36 ± 1.94	9.50 ± 0.36	29.17 ± 9.75
III	5.23 ± 2.46	17.40 ± 2.54	19.07 ± 10.68
IV	6.33 ± 2.62	15.10 ± 3.43	19.11 ± 8.72
V	6.58 ± 2.58	17.52 ± 8.66	10.06 ± 6.36

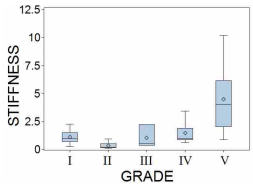

(a) Effect of degeneration on stiffness (N·m) in LB

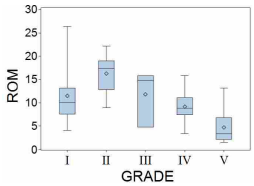

(b) Effect of degeneration on ROM (deg) in LB

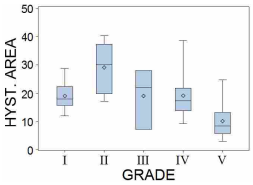

(c) Effect of degeneration on hysteresis area (N·m·deg) in LB

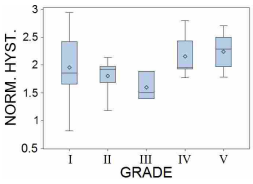

(d) Effect of degeneration on normalized hysteresis (N·m) in LB

Figure 3.8: These boxplots show the effect of degeneration on several parameters in lateral bending.

The effect of segment level on stiffness was statistically significant in AR and LB. Specifically, in both AR and LB, L5-S1 was significantly stiffer than L1-L2 and L3-L4. There was no statistically significant effect from segment level on stiffness in FE.

In both AR and LB, the decrease in ROM was statistically significant from L1-L2 and L3-L4 to L5-S1. There was no statistically significant effect from segment level on ROM in FE.

The effect of segment level on hysteresis area was statistically significant for AR and LB. In AR, the decrease in hysteresis area was significant from L1-L2 and L3-L4 to L5-S1. In LB, there was a statistically significant increase in hysteresis area from L1-L2 to L3-L4 and a statistically

Table 3.4: Means and standard deviations for normalized hysteresis according to grade of degeneration and listed by direction.

	Normalized Hysteresis (N·m)		
Grade	AR	FE	LB
I	1.31 ± 0.53	0.91 ± 0.01	1.95 ± 0.66
II	0.87 ± 0.35	0.97 ± 0.08	1.80 ± 0.37
III	1.49 ± 0.38	1.06 ± 0.14	1.59 ± 0.26
IV	1.35 ± 0.32	1.40 ± 0.26	2.15 ± 0.38
V	1.57 ± 0.40	1.85 ± 0.32	2.24 ± 0.30

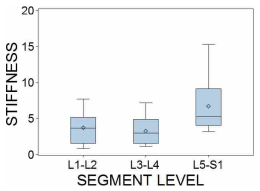

(a) Effect of segment level on stiffness (N·m) in AR

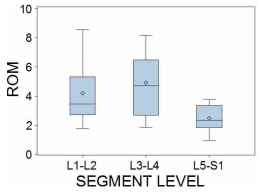

(b) Effect of segment level on ROM (deg) in AR

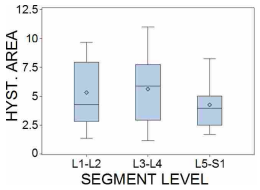

(c) Effect of segment level on hysteresis area (N·m·deg) in AR

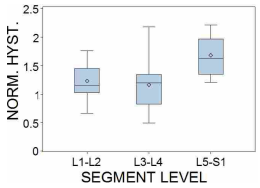

(d) Effect of segment level on normalized hysteresis (N·m) in AR

Figure 3.9: These boxplots show the effect of segment level on several parameters in axial rotation.

significant decrease from L3-L4 to L5-S1. The hysteresis area in L5-S1 is also significantly less than in L1-L2. There is a trend of increasing hysteresis area in FE, but no statistical significance.

The effect of segment level on normalized hysteresis was statistically significant in all three modes of loading. In AR, there is a statistically significant increase in normalized hysteresis from L3-L4 to L5-S1. In FE, normalized hysteresis increased from L1-L2 to L5-S1. In LB, the increase in normalized hysteresis was statistically significant from L1-L2 and L3-L4 to L5-S1.

Table 3.5: Means and standard deviations for the DIP-Boltzmann coefficients, listed by direction.

Parameter	AR	FE	LB
A (deg)	1.96 ± 1.06	5.49 ± 1.82	4.79 ± 3.03
B (deg)	1.96 ± 1.06	5.49 ± 1.82	4.79 ± 3.03
$m_{1,upper}$ (N·m)	-3.34 ± 1.02	-0.30 ± 1.28	-3.16 ± 1.53
$m_{2,upper}$ (N·m)	2.20 ± 1.27	1.17 ± 1.30	1.12 ± 1.36
$\alpha_{1,upper}$ $(1/\text{N·m})$	0.61 ± 0.12	1.32 ± 1.49	0.76 ± 0.61
$\alpha_{2,upper}$ $(1/\text{N·m})$	0.57 ± 0.10	1.93 ± 2.14	0.94 ± 1.19
$m_{1,lower}$ (N·m)	-1.95 ± 0.98	1.34 ± 1.04	-0.98 ± 1.47
$m_{2,lower}$ (N·m)	3.63 ± 1.13	2.60 ± 1.26	3.27 ± 1.49
$\alpha_{1,lower}$ $(1/\text{N·m})$	0.57 ± 0.13	2.31 ± 2.58	0.99 ± 1.28
$\alpha_{2,lower}$ $(1/\text{N·m})$	0.62 ± 0.13	1.18 ± 1.10	0.73 ± 0.35

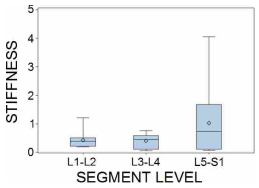

(a) Effect of segment level on stiffness (N·m) in FE

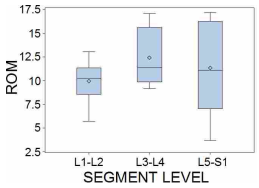

(b) Effect of segment level on ROM (deg) in FE

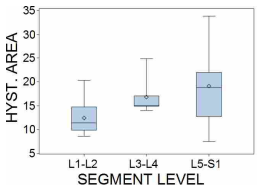

(c) Effect of segment level on hysteresis area (N·m·deg) in FE

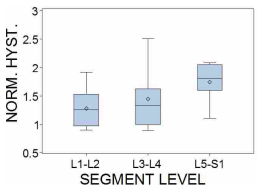

(d) Effect of segment level on normalized hysteresis (N·m) in FE

Figure 3.10: These boxplots show the effect of segment level on several parameters in flexion-extension.

3.3.3 Effect of Temperature

The FSUs were tested at body temperature (39 ± 2 °C) and room temperature (21 ± 1 °C). The statistical effects of temperature on stiffness, ROM, hysteresis area and normalized hysteresis are shown in Figure 3.12 for axial rotation, Figure 3.13 for flexion-extension, and Figure 3.14 for lateral bending.

The effect of temperature on stiffness was statistically significant in AR, with a reduced stiffness at body temperature.

Table 3.6: Summary of p-values obtained from the mixed model for the four parameters of interest in axial rotation, grouped by effect. Significant values for a confidence level of $\alpha = 0.05$ are indicated with an asterisk.

	Axial Rotation			
Parameter	Temp	Grade	Segment	Load
Stiffness (N·m)	0.0169*	< 0.0001*	< 0.0001*	< 0.0001*
ROM (deg)	0.0864	0.0004*	0.0001*	< 0.0001*
Hyst. Area (N·m·deg)	0.0013*	< 0.0001*	0.0049*	< 0.0001*
Norm. Hyst. (N·m)	0.0599	0.1353	0.0336*	0.0090*

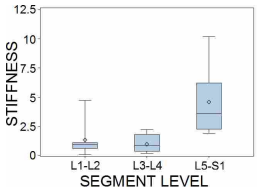

(a) Effect of segment level on stiffness (N·m) in LB

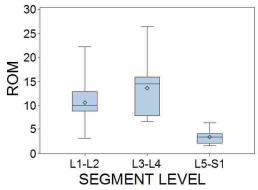

(b) Effect of segment level on ROM (deg) in LB

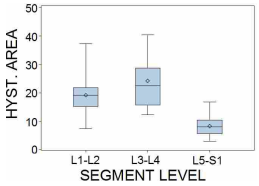

(c) Effect of segment level on hysteresis area (N·m·deg) in LB

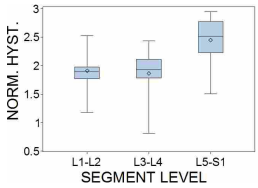

(d) Effect of segment level on normalized hysteresis (N·m) in LB

Figure 3.11: These boxplots show the effect of segment level on several parameters in lateral ending.

Testing at body temperature tended to increase ROM, but the effect was not statistically significant in any mode of loading.

Hysteresis area also generally increased at body temperature. The effect was statistically significant in AR and LB.

Normalized hysteresis generally increased at body temperature; the effect was marginally significant in AR, but it was not statistically significant in any mode of loading.

Table 3.7: Summary of p-values obtained from the mixed model for the four parameters of interest in flexion-extension, grouped by effect. Significant values for a confidence level of $\alpha = 0.05$ are indicated with an asterisk.

	Flexion-Extension			
Parameter	Temp	Grade	Segment	Load
Stiffness (N·m)	0.6194	0.4116	0.2790	0.3636
ROM (deg)	0.2583	0.0215*	0.7952	0.0046*
Hyst. Area (N·m·deg)	0.2882	0.8833	0.2454	0.3284
Norm. Hyst. (N·m)	0.2666	< 0.0001*	0.0200*	0.0003*

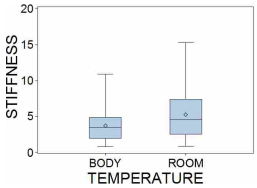

(a) Effect of temperature on stiffness (N·m) in AR

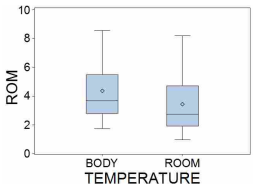

(b) Effect of temperature on ROM (deg) in AR

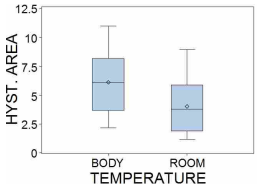

(c) Effect of temperature on hysteresis area (N·m·deg) in AR

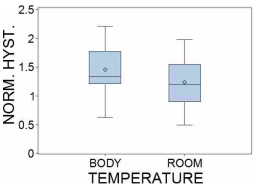

(d) Effect of temperature on normalized hysteresis (N·m) in AR

Figure 3.12: These boxplots show the effect of temperature on several parameters in axial rotation.

As stated previously, all of the results reported in this section were tested with a compressive follower load. When tested without a follower load, the increase in ROM at body temperature was statistically significant in ROM for FE and LB, and marginally significant in AR.

3.3.4 Effect of Follower Load

The results presented in this section include the testing performed on the 15 segments that were tested both with and without the 440 N compressive follower load. The statistical effects of the follower load on stiffness, ROM, hysteresis area and normalized hysteresis are shown in Figure 3.15 for axial rotation, Figure 3.16 for flexion-extension, and Figure 3.17 for lateral bending.

Table 3.8: Summary of p-values obtained from the mixed model for the four parameters of interest in lateral bending, grouped by effect. Significant values for a confidence level of $\alpha = 0.05$ are indicated with an asterisk.

	Lateral Bending			
Parameter	Temp	Grade	Segment	Load
Stiffness (N·m)	0.1881	0.0002*	$< 0.0001^*$	$< 0.0001^*$
ROM (deg)	0.1078	0.0018*	$< 0.0001^*$	$< 0.0001^*$
Hyst. Area (N·m·deg)	0.0235*	0.0012*	0.0001*	0.6798
Norm. Hyst. (N·m)	0.2753	0.1207	0.0017*	$< 0.0001^*$

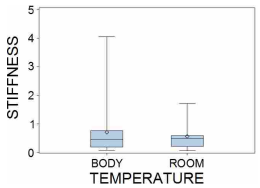

(a) Effect of temperature on stiffness (N·m) in FE

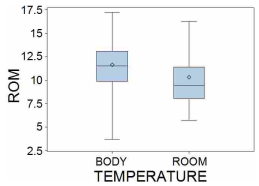

(b) Effect of temperature on ROM (deg) in FE

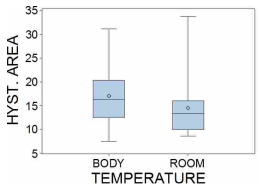

(c) Effect of temperature on hysteresis area (N·m·deg) in FE

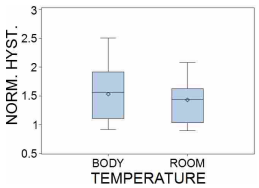

(d) Effect of temperature on normalized hysteresis (N·m) in FE

Figure 3.13: These boxplots show the effect of temperature on several parameters in flexion-extension.

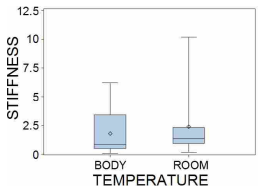

(a) Effect of temperature on stiffness (N·m) in LB

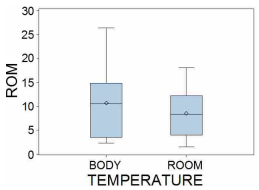

(b) Effect of temperature on ROM (deg) in LB

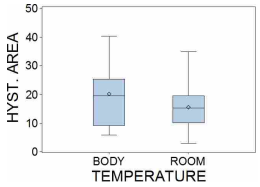

(c) Effect of temperature on hysteresis area (N·m·deg) in LB

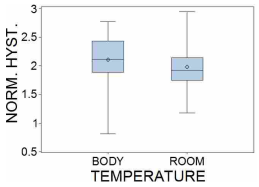

(d) Effect of temperature on normalized hysteresis (N·m) in LB

Figure 3.14: These boxplots show the effect of temperature on several parameters in lateral ending.

The follower load increased stiffness in all three modes of loading, but the effect was statistically significant only in AR and LB.

The follower load reduced ROM in all three modes of loading. The effect was statistically significant in all three.

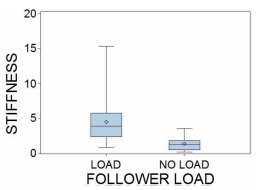

(a) Effect of follower load on stiffness (N·m) in AR

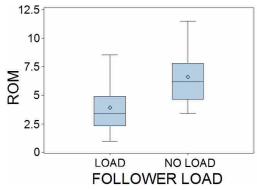

(b) Effect of follower load on ROM (deg) in AR

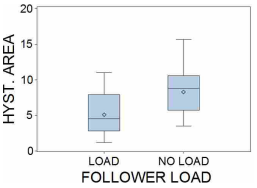

(c) Effect of follower load on hysteresis area (N·m·deg) in AR

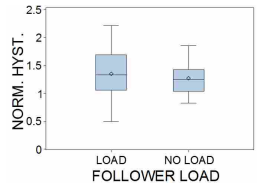

(d) Effect of follower load on normalized hysteresis (N·m) in AR

Figure 3.15: These boxplots show the effect of follower load on several parameters in axial rotation.

When the follower load was applied, hysteresis area was reduced in AR, but there was no statistically significant change in FE and LB.

Normalized hysteresis increased under the follower load. The effect was statistically significant in all three modes of loading.

It is also noteworthy that the statistical significance of the effects of segment level and degeneration were more pronounced in the presence of follower load than when there was no follower load.

3.3.5 Effect of Normalization

To account for differences in cross-sectional area of the intervertebral disc, the torque was normalized by CSA and by the area moment of inertia. The same statistical tests were run for these two cases as for the case of raw measured torque. Each of the four parameters are addressed and the notable differences in the statistical results due to normalization are listed below.

Neither normalizing by CSA nor by area moment affected the statistical results for stiffness or ROM in any mode of loading.

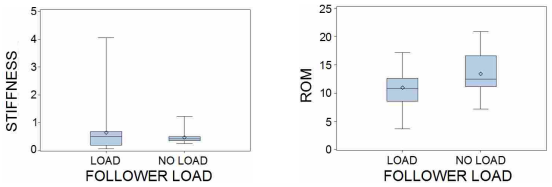

(a) Effect of follower load on stiffness (N·m) in FE

(b) Effect of follower load on ROM (deg) in FE

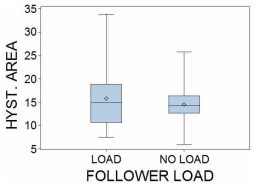

(c) Effect of follower load on hysteresis area (N·m·deg) in FE

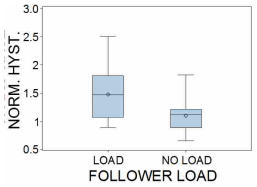

(d) Effect of follower load on normalized hysteresis (N·m) in FE

Figure 3.16: These boxplots show the effect of follower load on several parameters in flexion-extension.

The same was true for hysteresis area, with one exception. Normalizing by area moment caused the change in hysteresis area in FE to become statistically significant with respect to degeneration grade. It can also be noted that normalizing by CSA increased the statistical significance of hysteresis area in LB and normalizing by area moment decreased the statistical significance of hysteresis area in LB; however, the p-value was less than 0.05 for the raw torque as well as for both methods of normalization so the inferences based on the statistical results remain unchanged.

For normalized hysteresis, the statistical results were the same for raw measured torque as for both types of normalization, with the following exceptions: in AR, normalizing by CSA made the effect of degeneration grade not statistically significant; in FE, normalizing by CSA made the effects of grade and segment level not statistically significant; and in LB, normalizing by CSA again made the effect of segment level not statistically significant.

3.4 Discussion

There have been many studies showing the kinematic effects of degeneration [3, 23, 24, 26] but without the presence of a compressive follower load [14–18]. The results from the most relevant previous work are summarized and compared to the current study in Table 3.9. This

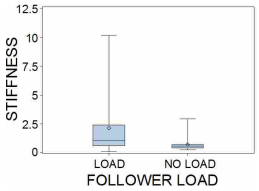

(a) Effect of follower load on stiffness (N·m) in LB

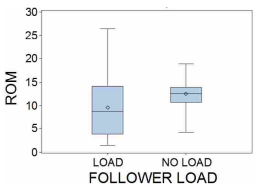

(b) Effect of follower load on ROM (deg) in LB

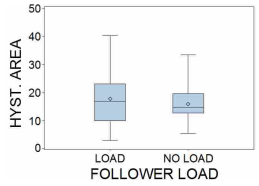

(c) Effect of follower load on hysteresis area (N·m·deg) in LB

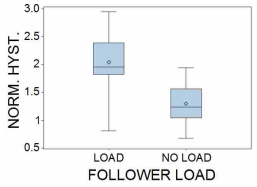

(d) Effect of follower load on normalized hysteresis (N·m) in LB

Figure 3.17: These boxplots show the effect of follower load on several parameters in lateral bending.

study evaluates the effects of degeneration on mobility under a compressive follower load. The DIP-Boltzmann sigmoid curve was used to fit the data, enabling the calculation and analysis of hysteresis in addition to ROM and stiffness. The study also looks briefly at the effect of temperature and follower load on lumbar spine segmental testing.

Table 3.9: The three studies with similar objectives [3, 23, 24] are summarized and compared to the current study. Legend: ROM is range of motion, NZ is neutral zone range, NZR is neutral zone ratio or NZ/ROM, K is stiffness, HA is hysteresis area, NH is normalized hysteresis, $*$ indicates statistical significance for $\alpha = 0.05$, † indicates a trend was identified, and — indicates that no data was reported for that loading direction.

Author	Year	FSUs	Age	Temp	Load	Rate	AR	FE	LB
Mimura	1994	47	35-64	Room	No	Step-wise	ROM† NZ* NZR*	ROM† NZ† NZR†	ROM† NZ NZR*
Krismer	2000	36	20-92	Room	No	Step-wise	ROM*	—	—
Tanaka	2001	114	39-87	Room	No	Step-wise	ROM*	ROM*	ROM*
Current Work	2011	21	46-100	Room Body	Yes	Continuous	ROM* K* HA* NH†	ROM† K* — NH*	ROM* K* HA* NH

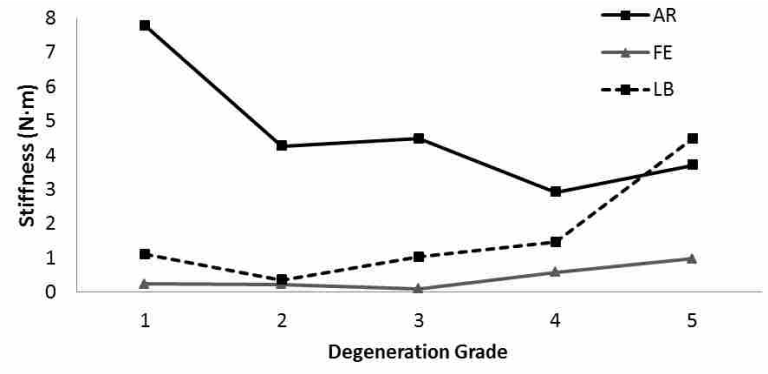

Figure 3.18: The mean stiffness for all segment levels at each grade of degeneration is shown for each direction of loading. The data for this plot is listed in Table 3.1.

3.4.1 Effect of Degeneration

The results generally support what has been suggested in previous studies. The trends of stiffness and ROM are not linear; both parameters also tend to have similar behavior in FE and LB, and the opposite in AR. Stiffness in AR tends to decrease rapidly in the initial stages of degeneration and increase slightly in advanced degeneration. Conversely, in FE and LB, stiffness tends to decrease slightly in the initial stages of degeneration and increase rapidly in advanced degeneration. These trends are illustrated in Figure 3.18, where the mean stiffness for each level of degeneration is plotted.

In ROM, the pattern is similar. In AR, ROM increases steadily from grades I to IV, but then tends to decrease at grade V. In FE and LB, ROM tends to increase initially and then decreases rapidly with continued degeneration. These trends are illustrated in Figure 3.19, where the mean range of motion for each level of degeneration is plotted.

This behavior can be explained by the histological effects of degeneration, especially as regarding the fibrocartilage breakdown in the annulus fibrosus. As the disc is weakened, there is less resistance to an axial torque. However, as the disc degenerates, there is a loss of hydration in addition to the loss of integrity in the fibrocartilage. Under a compressive load, therefore, the vertical disc space is reduced. Because rotations in flexion-extension and lateral bending both act in a direction that further compresses the disc, this causes an increase in stiffness and a decrease in ROM. The motion of the functional spinal unit is not due solely to the IVD; another factor that can account for increased ROM in AR is the reduced thickness of the articular cartilage on the

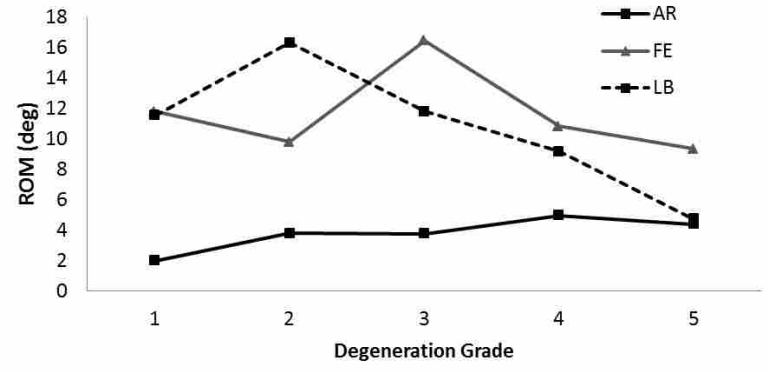

Figure 3.19: The mean range of motion for all segment levels at each grade of degeneration is shown for each direction of loading. The data for this plot is listed in Table 3.2.

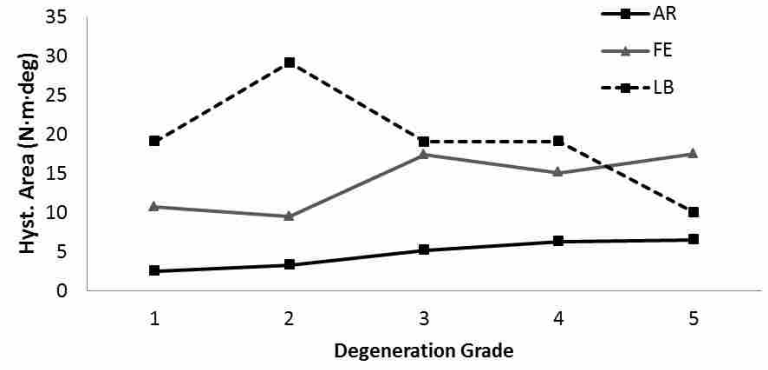

Figure 3.20: The mean hysteresis area for all segment levels at each grade of degeneration is shown for each direction of loading. The data for this plot is listed in Table 3.3.

zygopophyseal joints [61]. Physiological changes in ligaments may also play a role in increased joint laxity.

The changes in hysteresis area in FE are less definite, but the behavior in AR and LB are likely attributable to the same histological effects as stiffness and ROM. Hysteresis area consistently increases with degeneration in AR. In LB, hysteresis area increased from grade I to II, but then generally decreased with increasing degeneration. Again, these trends are illustrated in Figure 3.20.

Although the change in normalized hysteresis with degeneration was not statistically significant in AR or LB, there is a slight trend towards increasing normalized hysteresis with increasing degeneration. In FE, the same trend is apparent and is also statistically significant. These trends are illustrated in Figure 3.21.

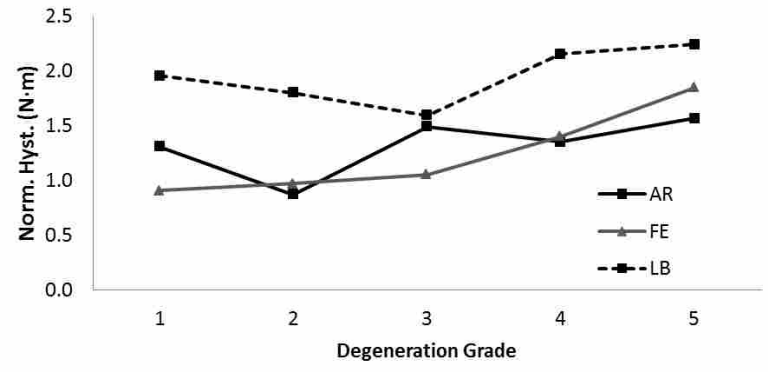

Figure 3.21: The mean normalized hysteresis for all segment levels at each grade of degeneration is shown for each direction of loading. The data for this plot is listed in Table 3.4.

3.4.2 Effect of Segment Level

Although it is not the primary goal of this research to evaluate the differences between segment levels, it is worth noting that the lumbosacral joint exhibited statistically different behavior in stiffness, ROM, and normalized hysteresis, though not in every mode of loading. This corresponds to the work done by Laud *et al.* [29]. Also of note is that two-thirds of the L5-S1 segments were in advanced stages of degeneration (grades IV and V), which may account for the increased stiffness and reduced range of motion.

3.4.3 Effect of Temperature

The effects of temperature were generally not statistically significant when tested with a compressive follower load; however, the trends indicate that temperature does have an effect on spine testing. It is recommended that these effects be considered when conducting similar tests. Ongoing research in the BYU Applied Biomechanics Engineering Laboratory (BABEL) will further analyze the effects of temperature on lumbar spine segmental testing.

3.4.4 Effect of Follower Load

An important indication of the effect of follower load is illustrated in the increase in joint laxity reported by Mimura *et al.* [3]. The increase in neutral zone ratio (NZ/ROM) is more pronounced when tested without a compressive follower load. While this furthers understanding of

the histological changes in the intervertebral disc with increasing degeneration, it does not necessarily represent the *in vivo* behavior associated with this physical change in the disc. Because of the loss of hydration and fiber integrity in advanced stages of degeneration, the intervertebral disc is more compressed and therefore stiffer in FE and LB (where the follower load compresses in the direction of rotation).

3.4.5 Effect of Normalization

In general, there was little difference in the results among the three approaches to normalization. Perhaps this is because the spines were specifically selected to be mostly females of a similar height (one male lumbar spine was included in the study). The height range was 61 to 67 in. The minimum CSA was 1263 mm and the maximum was 2689 mm. The statistical analysis performed can also account for the lack of effect seen when the data was normalized; in a repeated measures analysis of variance, the statistical error is isolated. The analysis, then, was effectually evaluating the magnitude of changes in a segment for the different effects (degeneration grade, segment level, temperature, and follower load) and comparing the changes to those of other segments.

3.4.6 Advantages of Standardized Curve Fit

A strong motivation for implementing a standard curve fit for spinal motion is to enable the comparison of data across studies. The model used in this paper, the DIP-Boltzmann sigmoid, has several advantages. One of the key features of this model is that each of the variables of the DIP-Boltzmann curve can be described physically (refer to Figure 3.5). Since A and B are the same for the upper and lower curve, a total of ten independent variables describe the entire response, including hysteresis.

Another advantage of the DIP-Boltzmann model is that it has a high coefficient of correlation to the raw data. As reported in Chapter 2, the average coefficient of correlation from fitting 63 torque-rotation curves was 0.9941.

The DIP-Boltzmann variables can be used to calculate all of the parameters of the torque-rotation curve of the lumbar spine which are analyzed in this work: stiffness, range of motion, hysteresis area, and normalized hysteresis.

3.4.7 Limitations of the Present Study

We were limited by the number of spines from which we were able to obtain data. We have tried to minimize any confounding variables by selecting spines that were physiologically similar.

Although care was taken to place the follower load so that it acted through the axis of rotation of the disc, the placement of the follower load could have induced an additional moment and augmented the rotation in FE. Additionally, the effect could be more pronounced in healthier discs because the axis of rotation translates more in healthier discs than degenerated discs.

During testing, it became evident that the FSU was very sensitive to follower load placement, especially in FE. In our test setup, the follower load was placed along the A-A axis shown in Figure 3.4. This was acceptable for LB, as the direction of rotation was perpendicular to the follower load. However, in FE, the rotation occurred about the same axis (A-A). If the follower load was not perfectly aligned with that axis of rotation, or if the center of rotation of the disc translated during testing, the follower load would induce an additional and undesirable moment on the system. This would result in exaggerated rotations for both flexion and extension. We therefore recommend that the follower load always be placed perpendicular to the axis of rotation. Axial rotation occurs about an axis perpendicular to both A-A and B-B, so it is much less sensitive to follower load placement.

Because of the difficulty with the follower load placement, we excluded the first 6 FSUs from the analysis in FE. As a result, we were particularly lacking healthy specimens for that analysis. The smaller sample size reduces the power for the statistical tests; it is probable that with a larger sample size, we would find more statistical significance in FE.

3.4.8 Implant Design or Clinical Relevance

This research associates segmental mechanical response with intervertebral disc degeneration under physiologic testing conditions. By correlating the torque-rotation response with the

level of degeneration, devices can be designed to an appropriate range of motion and stiffness, potentially reducing the impact on adjacent discs [4].

3.5 Acknowledgments

The authors acknowledge the support from the BYU Applied Biomechanics Engineering Laboratory and Compliant Mechanisms Research Group. We also gratefully acknowledge our funding sources, Crocker Spinal Technologies, Inc. and the BYU Technology Transfer Office.

The assistance of Dennis L. Eggett from the BYU Department of Statistics for consultation on the statistical analysis is gratefully acknowledged.

CHAPTER 4. CONCLUSIONS AND RECOMMENDATIONS

4.1 Summary of Contributions

This thesis contributes useful knowledge regarding the effects of degeneration on lumbar segment mobility and also provides the DIP-Boltzmann model as a useful tool for analyzing spinal rotations.

There have been many studies showing the kinematic effects of degeneration [3, 23, 24, 26] and other studies have analyzed the effect of and need for a compressive follower load [14–18]. This study evaluated the effects of degeneration on mobility under a compressive follower load. The DIP-Boltzmann sigmoid curve was used to fit the data, enabling the calculation and analysis of hysteresis in addition to ROM and stiffness. The study also briefly evaluated the effect of temperature and follower load on lumbar spine segmental testing.

This thesis has presented the DIP-Boltzmann sigmoid curve as a favorable model for the torque-rotation response of the human lumbar spine. The curve fit parameters have physical meaning (e.g., range of motion and boundaries of neutral zone), and other important characteristics (e.g., stiffness of neutral zone and hysteresis) can be directly calculated from them.

A key contribution of this curve fit is the possibility of comparing data across studies. This is especially beneficial when considering the high costs of cadaveric testing. The parameters of the model will also provide input to the development process of creating devices with the same motion response as that exhibited by the spine.

The DIP-Boltzmann equation is of particular significance for implant design. The device can be modeled so that the implant has the full sigmoidal behavior with accurate range of motion and stiffness, rather than only reproducing discrete points of natural segmental response. Spinal implant design is improved by eliminating discontinuities in the response; using the DIP-Boltzmann model as a design tool can help accomplish this objective.

This thesis has also presented the results from testing of 21 functional spinal units (FSUs). The full set of DIP-Boltzmann model coefficients for the data collected in this study are included in Appendix A. The effect of degeneration was statistically significant ($\alpha = 0.05$) for stiffness, ROM, and hysteresis area in axial rotation (AR) and lateral bending (LB); it was also statistically significant for ROM and normalized hystersis in flexion-extension (FE). The lumbosacral joint (L5-S1) was significantly stiffer in AR and LB; the decrease in ROM and hysteresis area in AR and LB were also statistically significant for the lumbosacral joint compared to L1-L2 and L3-L4. Temperature had a significant effect on stiffness and hysteresis area in AR and on hysteresis area in LB. The follower load increased stiffness in all three modes of loading, but was significant only in AR and LB; it also reduced ROM and increased normalized hysteresis in all three modes of loading.

The results from this testing increase understanding about the effects of degeneration on spinal biomechanics. Because the testing was conducted under physiologic conditions (including a compressive follower load and at body temperature), the cadaveric segmental response more closely matches the *in vivo* response. The testing results can also be used to validate other mathematical and engineering models of the lumbar spine, including finite element models.

4.2 Recommendations for Future Work

To better understand and accurately interpret the motion of the lumbar FSU, more testing is needed, particularly in FE. Although care was taken to place the follower load so that it acted through the axis of rotation of the FSU, the placement of the follower load could have induced an undesired moment and augmented the rotation in both flexion and extension. Additionally, the effect could be more pronounced in healthier discs because the axis of rotation translates more in healthier discs than degenerated discs. Because of the difficulty with the follower load placement, we excluded the first 6 FSUs from the analysis in FE. As a result, we were particularly lacking healthy specimens for that analysis. The smaller sample size reduces the power for the statistical tests; it is probable that with a larger sample size, we would find more statistical significance in FE.

4.2.1 Follower Load Placement

During testing, it became evident that the FSU was sensitive to follower load placement, especially in FE. In our test setup, the follower load was placed along the A-A axis shown in Figure 3.4. This was acceptable for LB, as the direction of rotation was perpendicular to the follower load. However, in FE, the rotation occurred about the same axis (A-A). If the follower load was not perfectly aligned with that axis of rotation, or if the center of rotation of the disc translated during testing, the follower load would induce an additional and undesirable moment on the system. This would result in exaggerated rotations for both flexion and extension. We therefore recommend that the follower load always be placed perpendicular to the axis of rotation. Axial rotation occurs about an axis perpendicular to both A-A and B-B, so it is much less sensitive to follower load placement.

A better methodology needs to be developed for the application of a follower load in spine segment testing. Proper alignment with the axis of rotation is only one aspect to be addressed. It is still unknown what weight the follower load should be for testing single-level or multi-level FSUs. Patwardhan *et al.* [15] have made some progress in defining the path of the follower load through each level of the lumbar spine, but there is still room for improvement in that area as well.

4.2.2 Temperature Testing

Although the effects of temperature were generally not statistically significant when tested with a compressive follower load, the trends indicate that temperature does have an effect on spine testing. While ongoing research in the BYU Applied Biomechanics Engineering Laboratory (BABEL) will further analyze the effects of temperature, it is recommended that this research be pursued further.

4.2.3 Implant Design

This research associates segmental mechanical response with intervertebral disc degeneration under physiologic testing conditions. By correlating the torque-rotation response with the level of degeneration, devices can be designed to an appropriate range of motion and stiffness, potentially reducing the impact on adjacent discs [4]. An example application is the FlexSuRe™.

There are several potential approaches to this problem. If the FlexSuRe is intended to provide decompression for a grade III or IV to stimulate regeneration, then data collected without a follower load may help in developing the design criteria.

4.2.4 DIP-Boltzmann Sigmoid

For the DIP-Boltzmann sigmoid model, because we chose to constrain A and B and allowed m_1 and m_2 to be set by the model, the neutral zone was not always clearly demarcated. Further research could identify a more robust way to apply the DIP-Boltzmann curve fit such that m_1 and m_2 more closely match the inflection points of the curve.

REFERENCES

[1] S. A. Zirbel, D. K. Stolworthy, A. E. Bowden, and L. L. Howell, "Standardized characterization of lumbar segmental response using a dual inflection point boltzmann sigmoid," *International Journal for Numerical Methods in Biomedical Engineering*, 2011. 1, 7

[2] F. Knutsson, "The instability associated with disc degeneration in the lumbar spine," *Acta Radiol*, vol. 25, pp. 593–608, 1944. 1, 19

[3] M. Mimura, M. M. Panjabi, T. R. Oxland, J. J. Crisco, I. Yamamoto, and A. Vasavada, "Disc degeneration affects the multidirectional flexibility of the lumbar spine," *Spine*, vol. 19, no. 12, pp. 1371–1380, 1994. 1, 4, 9, 10, 19, 24, 39, 40, 43, 47

[4] I. A. F. Stokes and J. C. Iatridis, "Mechanical conditions that accelerate intervertebral disc degeneration: overload versus immobilization," *Spine*, vol. 29, pp. 2724–2732, 2004. 1, 19, 20, 46, 49

[5] J. C. Iatridis, P. L. Mente, I. A. F. Stokes, D. D. Aronsson, and M. Alini, "Compression-induced changes in intervertebral disc properties in a rat tail model," *Spine*, vol. 24, no. 10, pp. 996–1002, 1999. 1, 19

[6] M. A. Adams and P. J. Roughley, "What is intervertebral dis degeneration, and what causes it?" *Spine*, vol. 31, no. 18, pp. 2151–2161, 2006. 1, 3, 19

[7] M. Solomonow, E. Eversull, B. H. Zhou, R. V. Baratta, and M.-P. Zhu, "Neuromuscular neutral zones associated with viscoelastic hysteresis during cyclic lumbar flexion," *Spine*, vol. 26, no. 14, pp. E314–E324, 2001. 2, 8

[8] J.-L. Wang, M. Parianpour, A. Shirazi-Adl, and A. E. Engin, "Viscoelastic finite-element analysis of a lumbar motion segment in combined compression and sagittal flexion," *Spine*, vol. 25, no. 3, pp. 310–318, 2000. 2, 8

[9] M. D. Humzah and R. W. Soames, "Human intervertebral disc: Structure and function," *The Anatomical Record*, vol. 220, no. 4, pp. 337–356, 1988. 2, 3, 8

[10] M. M. Panjabi, "The stabilizing system of the spine. part ii. neutral zone and instability hypothesis," *Journal of Spinal Disorders*, vol. 5, no. 4, pp. 390–397, 1992. 2, 8

[11] N. R. Crawford, J. D. Peles, and C. A. Dickman, "The spinal lax zone and neutral zone: Measurement techniques and parameter comparisons," *Journal of Spinal Disorders and Techniques*, vol. 11, no. 5, pp. 416–429, 1998. 2, 8

[12] N. Boos, S. Weissbach, H. Rohrbach, C. Weiler, K. F. Spratt, and A. G. Nerlich, "Classification of the age-related changes in lumbar intervertebral discs," *Spine*, vol. 27, no. 23, pp. 2631–2644, 2002. 3

[13] J. P. G. Urban and C. P. Winlove, "Pathophysiology of the intervertebral disc and the challenges for mri," *Journal of Magnetic Resonance Imaging*, vol. 25, pp. 419–432, 2007. 3

[14] A. G. Patwardhan, R. M. Havey, K. P. Meade, B. Lee, and B. Dunlap, "A follower load increases the load-carrying capacity of the lumbar spine in compression," *Spine*, vol. 24, no. 10, pp. 1003–1009, 1999. 3, 39, 47

[15] A. G. Patwardhan, R. M. Havey, G. Carandang, J. Simonds, L. I. Voronov, A. J. Ghanayem, K. P. Meade, T. M. Gavin, and O. Paxinos, "Effect of compressive follower preload on the flexion-extension response of the human lumbar spine," *Journal of Orthopaedic Research*, vol. 21, pp. 540–546, 2003. 3, 9, 22, 39, 47, 49

[16] A. G. Patwardhan, K. P. Meade, and B. Lee, "A frontal plane model of the lumbar spine subjected to a follower load: Implications for the role of muscles," *Journal of Biomechanical Engineering*, vol. 123, pp. 212–217, 2001. 3, 39, 47

[17] S. M. Renner, R. N. Natarajan, A. G. Patwardhan, R. M. Havey, L. I. Voronov, B. Y. Guo, G. B. J. Andersson, and H. S. An, "Novel model to analyze the effect of a large compressive follower pre-load on range of motions in a lumbar spine," *J Biomechanics*, vol. 40, pp. 1326–1332, 2007. 3, 10, 39, 47

[18] A. Rohlmann, T. Zander, M. Rao, and G. Bergmann, "Applying a follower load delivers realistic results for simulating standing," *Journal of Biomechanics*, vol. 42, no. 10, pp. 1520–1526, 2009. 3, 39, 47

[19] K.-S. Han, A. Rohlmann, S.-J. Yang, B. S. Kim, and T.-H. Lim, "Spinal muscles can create compressive follower loads in the lumbar spine in a neutral standing posture," *Medical Engineering and Physics*, vol. 33, no. 4, pp. 472–478, 2011. 3

[20] J. P. Thompson, R. H. Pearce, M. T. Schechter, M. E. Adams, I. K. Y. Tsang, and P. B. Bishop, "Preliminary evaluation of a scheme for grading the gross morphology of the human intervertebral disc," *Spine*, vol. 15, pp. 411–415, 1990. 4, 19, 24

[21] M. Haefeli, F. Kalberer, D. Saegesser, A. G. Nerlich, N. Boos, and G. Paesold, "The course of macroscopic degeneration in the human lumbar intervertebral disc," *Spine*, vol. 31, no. 14, pp. 1522–1531, 2006. 4

[22] L. M. Benneker, P. F. Heini, S. E. Anderson, M. Alini, and K. Ito, "Correlation of radiographic and mri parameters to morphological and biochemical assessment of intervertebral disc degeneration," *Eur Spine J*, vol. 14, no. 1, pp. 27–35, 2005. 4

[23] N. Tanaka, H. S. An, T.-H. Lim, A. Fujiwara, C.-H. Jeon, and V. M. Haughton, "The relationship between disc degeneration and flexibility of the lumbar spine," *The Spine Journal*, vol. 1, pp. 47–56, 2001. 4, 5, 19, 39, 40, 47

[24] M. Krismer, C. Haid, H. Behensky, P. Kapfinger, F. Landauer, and F. Rachbauer, "Motion in lumbar functional spine units during side bending and axial rotation moments depending on the degree of degeneration," *Spine*, vol. 25, no. 16, pp. 2020–2027, 2000. 4, 10, 19, 39, 40, 47

[25] C. Quack, P. Schenk, T. Laeubli, S. Spillmann, J. Hodler, B. A. Michel, and A. Klipstein, "Do mri findings correlate with mobility tests? an explorative analysis of the test validity with regard to structure," *Eur Spine J*, vol. 16, pp. 803–812, 2007. 4

[26] A. Fujiwara, T.-H. Lim, H. S. An, N. Tanaka, C.-H. Jeon, G. B. J. Andersson, and V. M. Haughton, "The effect of disc degeneration and facet joint osteoarthritis on the segmental flexibility of the lumbar spine," *Spine*, vol. 25, no. 23, pp. 3036–3044, 2000. 5, 10, 24, 39, 47

[27] A. L. Nachemson, A. B. Schultz, and M. H. Berkson, "Mechanical properties of human lumbar spine motion segments: Influences of age, sex, disc level, and degeneration," *Spine*, vol. 4, no. 1, pp. 1–8, 1979. 5, 24

[28] I. Yamamoto, M. M. Panjabi, T. Crisco, and T. Oxland, "Three-dimensional movements of the whole lumbar spine and lumbosacral joint," *Spine*, vol. 14, no. 11, pp. 1256–1260, 1989. 5

[29] Y. Guan, N. Yoganandan, J. Moore, F. A. Pintar, J. Zhang, D. J. Maiman, and P. Laud, "Moment-rotation responses of the human lumbosacral spinal column," *J Biomechanics*, vol. 40, pp. 1975–1980, 2007. 5, 20, 43

[30] A. E. Bowden, H. L. Guerin, M. L. Villarraga, A. G. Patwardhan, and J. A. Ochoa, "Quality of motion considerations in numerical analysis of motion restoring implants of the spine," *Clinical Biomechanics*, vol. 23, pp. 536–544, 2008. 7, 20

[31] M. M. Panjabi, M. Krag, D. Summers, and T. Videman, "Biomechanical time-tolerance of fresch cadaveric human spine specimens," *Journal of Orthopedic Research*, vol. 3, pp. 292–300, 1985. 9, 20

[32] D. J. Goertzen, C. Lane, and T. R. Oxland, "Neutral zone and range of motion in the spine are greater with stepwise loading than with a continuous loading protocol. an in vitro porcine investigation," *Journal of Biomechanics*, vol. 37, no. 2, pp. 257–261, 2004. 9, 22

[33] D. S. Pflaster, M. H. Krag, C. C. Johnson, L. D. Haugh, and M. H. Pope, "Effect of test environment on intervertebral disc hydration," *Spine*, vol. 22, pp. 1133–1139, 1997. 9, 22

[34] D. K. Stolworthy, S. A. Zirbel, M. A. Samuels, A. E. Bowden, and L. L. Howell, "Increased loading rate decreases hysteresis and rom in the human lumbar spine," in *ORS Conference Proceedings*, 2011. 9, 22

[35] H.-J. Wilke, K. Wenger, and L. Claes, "Testing criteria for spinal implants: recommendations for the standardization of in vitro stability testing of spinal implants," *Eur Spine J*, vol. 7, pp. 148–154, 1998. 9, 19, 22

[36] A. Rohlmann, S. Neller, L. Claes, G. Bergmann, and H.-J. Wilke, "Influence of a follower load on intradiscal pressure and intersegmental rotation of the lumbar spine," *Spine*, vol. 26, no. 24, pp. E557–E561, 2001. 9, 22

[37] V. K. Goel, D. G. Wilder, M. H. Pope, and W. T. Edwards, "Controversy biomechanical testing of the spine. loadcontrolled versus displacement-controlled analysis." *Spine*, vol. 20, pp. 2354–2357, 1995. 9, 22

[38] M. M. Panjabi, I. Yamamoto, T. R. Oxland, and J. J. Crisco, "How does posture affect coupling in the lumbar spine?" *Spine*, vol. 14, pp. 1002–1011, 1989. 9, 10, 24

[39] T. R. Oxland, J. J. Crisco, M. M. Panjabi, and I. Yamamoto, "The effect of injury on rotational coupling at the lumbosacral joint," *Spine*, vol. 17, pp. 74–80, 1992. 9, 10, 24

[40] C. A. Niosi and T. R. Oxland, "Degenerative mechanics of the lumbar spine," *The Spine Journal*, vol. 4, pp. 202S–208S, 2004. 10

[41] M. M. Panjabi, T. R. Oxland, I. Yamamoto, and J. J. Crisco, "Mechanical behavior of the human lumbar and lumbosacral spine as shown by three-dimensional load-displacement curves," *JBJS*, vol. 76, pp. 413–424, 1994. 10

[42] J. S. Petrick, B. Jagadish, E. A. Mash, and H. V. Aposhian, "Monomethylarsonous acid (mma-iii) and arsenite: Ld50 in hamsters and in vitro inhibition of pyruvate dehydrogenase," *Chemical Research in Toxicology*, vol. 14, no. 6, pp. 651–656, 2001. 12

[43] F. Ginanneschi, F. D. Santo, F. Dominici, F. Gelli, R. Mazzocchio, and A. Rossi, "Changes in corticomotor excitability of hand muscles in relation to static shoulder positions," *Experimental Brain Research*, vol. 161, no. 3, pp. 374–382, 2004. 12

[44] B. Kalbfuss, A. Knochlein, T. Krober, and U. Reichl, "Monitoring influenza virus content in vaccine production: Precise assays for the quantitation of hemagglutination and neuraminidase activity," *Biologicals*, vol. 36, pp. 145–161, 2008. 12

[45] V. Gajendiram and M. L. Buist, "A quantitative description of active force generation in gastrointestinal smooth muscle," *International Journal for Numerical Methods in Biomedical Engineering*, vol. 27, pp. 450–460, 2011. 12

[46] K. Hemalatha and M. Manivannan, "Cardiopulmonary model to study interaction hemodynamics in muller maneuver," *International Journal for Numerical Methods in Biomedical Engineering*, vol. 27, 2011. 12

[47] B. J. Love, F. P. Ruinet, and F. Teyssandier, "Chemorheology of photopolymerizable acrylates using a modified boltzmann sigmoidal model," *Journal of Polymer Science Part B: Polymer Physics*, vol. 46, pp. 2319–2325, 2008. 12

[48] B. J. Love, F. Teyssandier, Y. Y. Sun, and C. P. Wong, "Sigmoidal chemorheological models of chip-underfill materials offer alternative predictions of combined cure and flow," *Macromolecular Materials and Engineering*, vol. 293, pp. 832–835, 2008. 12

[49] M. Elmquist, G. Corelissen, Z. Kukulska, and O. Gustafsson, "Distinct oxidative stabilities of char versus soot black carbon: Implications for quantification and environmental recalcitrance," *Global Biogeochemical Cycles*, vol. 20, pp. 1–11, 2006. 12

[50] T. S. Carey, A. T. Evans, and N. M. Hadler, "Acute severe low back pain: A population-based study of prevalence and care-seeking," *Spine*, vol. 21, pp. 339–344, 1996. 20

[51] "Nonfatal occupational injuries and illnesses requiring days away from work," Bureau of Labor Statistics, Tech. Rep., 2009. 20

[52] K. Luoma, H. Riihimaki, R. Luukkonen, R. Raininko, E. Viikari-Juntura, and A. Lamminen, "Low back pain in relation to lumbar disc degeneration," *Spine*, vol. 25, pp. 487–492, 2000. 20

[53] B. W. Cunningham, J. D. Gordon, A. E. Dmitriev, N. Hu, and P. C. McAfee, "Biomechanical evaluation of total disc replacement arthroplasty: an in vitro human cadaveric model," *Spine*, vol. 28, pp. S110–S117, 2003. 23

[54] T. Yoshioka, H. Tsuji, N. Hirano, and S. Sainoh, "Motion characteristic of the normal lumbar spine in young adults: instantaneous axis of rotation and vertebral center motion analyses," *Journal of Spinal Disorders*, vol. 3, pp. 103–113, 1990. 23

[55] H. L. Guerin and D. M. Elliott, "Load-induced fiber reorientation of human annulus fibrosus: influence on mechanics and the effect of degeneration," in *Transactions of the Orthopaedic Research Society*, vol. 30, 2005, p. 1585. 24

[56] D. G. Candow and P. D. Chilibeck, "Differences in size, strength, and power of upper and lower body muscle groups in young and older men," *Journal of Gerontology: Biological Sciences*, vol. 60A, no. 2, pp. 148–156, 2005. 24

[57] C. S. Bickel, J. K. Petrella, and G. A. Dudley, "Normalized torque of the quadriceps femoris is similar between active old and young adults," *Medicine and Science in Sports and Exercise*, vol. 36, no. 5, p. S357, 2004. 24

[58] S. Mathur, D. L. MacIntyre, B. B. Forster, and W. D. Reid, "Influence of exercise-induced injury on knee extension torque in the presence of long-standing quadriceps atrophy: case report," *Physiotherapy Canada*, vol. 57, no. 4, pp. 305–313, 2005. 24

[59] R. C. Hibbeler, *Engineering Mechanics: Statics*, 8th ed. Prentice-Hall, 1998. 24

[60] W. D. Pilkey, *Analysis and Design of Elastic Beams*. John Wiley and Sons, Inc, 2002. 25

[61] M. A. Adams, N. Bogduk, K. Burton, and P. Dolan, *The Biomechanics of Back Pain*, 2nd ed. Churchill Livingstone, 2006. 42

APPENDIX A. DIP-BOLTZMANN PARAMETERS

A.1 List of DIP-Boltzmann Parameters

The coefficients for the DIP-Boltzmann model for all data collected are listed in Tables A.1 to A.21. For this regression model, the coefficients A and B were constrained to be the minimum and maximum rotations of the lumbar spine, respectively. The torque-rotation curves were centered before the curve fit was applied so that A and B are equal.

Table A.1: List of DIP-Boltzmann parameters for spine C070369, segment L1-L2.

Spine	Segment	Grade	Direction	Temp	Load	Curve	A	B	α_1	m_1	α_2	m_2
C070369	L1-L2	I	AR	Body	Load	Upper	-1.3410	1.3410	0.6296	-3.8182	0.5567	2.8606
C070369	L1-L2	I	AR	Body	Load	Lower	-1.3410	1.3410	0.5547	-2.5430	0.5327	3.8690
C070369	L1-L2	I	AR	Room	Load	Upper	-0.8811	0.8811	0.6307	-3.8905	0.5633	2.6368
C070369	L1-L2	I	AR	Room	Load	Lower	-0.8811	0.8811	0.5889	-2.6444	0.5889	3.8859
C070369	L1-L2	I	AR	Body	No Load	Upper	-2.2677	2.2677	0.5131	-2.0672	0.5196	1.1476
C070369	L1-L2	I	AR	Body	No Load	Lower	-2.2677	2.2677	0.5753	-1.3971	0.5161	3.2664
C070369	L1-L2	I	AR	Room	No Load	Upper	-1.7018	1.7018	0.5341	-2.6645	0.5697	1.7250
C070369	L1-L2	I	AR	Room	No Load	Lower	-1.7018	1.7018	0.5963	-1.8370	0.5475	3.1510
C070369	L1-L2	I	FE	Body	Load	Upper	-6.0929	6.0929	3.0461	0.6861	0.4753	1.1596
C070369	L1-L2	I	FE	Body	Load	Lower	-6.0929	6.0929	3.3730	1.1672	0.6279	2.5013
C070369	L1-L2	I	FE	Room	Load	Upper	-5.7031	5.7031	3.0438	0.0507	0.6032	0.9193
C070369	L1-L2	I	FE	Room	Load	Lower	-5.7031	5.7031	2.5277	0.7126	0.5874	2.1051
C070369	L1-L2	I	FE	Body	No Load	Upper	-6.0559	6.0559	0.4278	0.5047	1.2072	1.2417
C070369	L1-L2	I	FE	Body	No Load	Lower	-6.0558	6.0558	1.0936	1.2620	0.4702	2.0553
C070369	L1-L2	I	FE	Room	No Load	Upper	-5.5877	5.5877	0.4600	0.6628	1.2972	1.3728
C070369	L1-L2	I	FE	Room	No Load	Lower	-5.5877	5.5877	1.1700	1.4590	0.4769	1.9624
C070369	L1-L2	I	LB	Body	Load	Upper	-5.0325	5.0325	0.7225	-3.8104	0.8954	1.1215
C070369	L1-L2	I	LB	Body	Load	Lower	-5.0325	5.0325	0.5846	-1.1389	0.6083	2.3580
C070369	L1-L2	I	LB	Room	Load	Upper	-4.4073	4.4073	0.5357	-3.1489	0.7933	1.0972
C070369	L1-L2	I	LB	Room	Load	Lower	-4.4073	4.4073	0.8263	-1.0450	0.7267	2.6380
C070369	L1-L2	I	LB	Body	No Load	Upper	-6.2945	6.2945	0.3873	-1.8416	0.9802	0.2851
C070369	L1-L2	I	LB	Body	No Load	Lower	-6.2945	6.2945	1.1037	0.0352	0.3643	0.7269
C070369	L1-L2	I	LB	Room	No Load	Upper	-5.4672	5.4672	1.1495	-0.0115	0.3752	-0.8936
C070369	L1-L2	I	LB	Room	No Load	Lower	-5.4672	5.4672	1.1867	0.0506	0.3860	0.7363

Table A.2: List of DIP-Boltzmann parameters for spine C070369, segment L3-L4.

Spine	Segment	Grade	Direction	Temp	Load	Curve	A	B	α_1	m_1	α_2	m_2
C070369	L3-L4	I	AR	Body	Load	Upper	-1.3379	1.3379	0.4834	-3.5398	0.5235	2.3391
C070369	L3-L4	I	AR	Body	Load	Lower	-1.3379	1.3379	0.4025	-1.6935	0.5069	3.368
C070369	L3-L4	I	AR	Room	Load	Upper	-0.9525	0.9525	0.3824	-1.0155	0.4381	0.5781
C070369	L3-L4	I	AR	Room	Load	Lower	-0.9525	0.9525	0.4209	-1.0808	0.4443	1.9856
C070369	L3-L4	I	FE	Body	Load	Upper	-1.8788	1.8788	0.5018	-3.1727	0.6627	5.3557
C070369	L3-L4	I	FE	Body	Load	Lower	-1.8788	1.8788	0.4547	-0.7371	1.6816	6.6530
C070369	L3-L4	I	FE	Room	Load	Upper	-1.6771	1.6771	0.4408	-1.9419	1.5896	6.6197
C070369	L3-L4	I	FE	Room	Load	Lower	-1.6771	1.6771	0.4124	-0.5200	3.5909	6.9637
C070369	L3-L4	I	LB	Body	Load	Upper	-5.2945	5.2945	0.8055	-2.6252	0.4356	0.7620
C070369	L3-L4	I	LB	Body	Load	Lower	-5.2945	5.2945	0.7156	-0.8415	0.5404	3.5018
C070369	L3-L4	I	LB	Room	Load	Upper	-5.1207	5.1207	0.3846	-0.7941	1.4581	3.0740
C070369	L3-L4	I	LB	Room	Load	Lower	-5.1207	5.1207	0.4081	1.0472	1.7935	4.5994

Table A.3: List of DIP-Boltzmann parameters for spine C070369, segment L5-S1.

Spine	Segment	Grade	Direction	Temp	Load	Curve	A	B	α_1	m_1	α_2	m_2
C070369	L5-S1	I	AR	Body	Load	Upper	-0.8644	0.8644	0.5006	-6.0748	0.4062	3.0327
C070369	L5-S1	I	AR	Body	Load	Lower	-0.8644	0.8644	0.3666	-5.0671	0.6213	4.2884
C070369	L5-S1	I	AR	Room	Load	Upper	-0.4829	0.4829	0.6657	-4.4607	0.5437	2.7263
C070369	L5-S1	I	AR	Room	Load	Lower	-0.4829	0.4829	0.4720	-2.8583	0.6486	5.2625
C070369	L5-S1	I	FE	Body	Load	Upper	-4.3405	4.3405	0.5257	-1.8298	0.8294	3.1204
C070369	L5-S1	I	FE	Body	Load	Lower	-4.3405	4.3405	0.5008	2.1845	1.1400	4.6975
C070369	L5-S1	I	FE	Room	Load	Upper	-3.3349	3.3349	0.2140	-6.5047	1.2808	3.0179
C070369	L5-S1	I	FE	Room	Load	Lower	-3.3349	3.3349	0.4903	2.5918	1.8273	5.6535
C070369	L5-S1	I	LB	Body	Load	Upper	-3.1490	3.1490	0.4295	-2.6418	1.0691	2.7574
C070369	L5-S1	I	LB	Body	Load	Lower	-3.1490	3.1490	0.4005	1.0141	1.6453	4.7697
C070369	L5-S1	I	LB	Room	Load	Upper	-2.0385	2.0385	0.5472	-2.1863	0.8243	1.7868
C070369	L5-S1	I	LB	Room	Load	Lower	-2.0385	2.0385	0.4492	2.2691	1.3572	3.4844

Table A.4: List of DIP-Boltzmann parameters for spine C090519, segment L1-L2.

Spine	Segment	Grade	Direction	Temp	Load	Curve	A	B	α_1	m_1	α_2	m_2
C090519	L1-L2	IV	AR	Body	Load	Upper	-1.7138	1.7138	0.6478	-4.0807	0.5674	2.3180
C090519	L1-L2	IV	AR	Body	Load	Lower	-1.7138	1.7138	0.5609	-2.6803	0.6119	3.6866
C090519	L1-L2	IV	AR	Room	Load	Upper	-1.4203	1.4203	0.6229	-3.7847	0.5869	2.4695
C090519	L1-L2	IV	AR	Room	Load	Lower	-1.4203	1.4203	0.5772	-2.649	0.6001	3.6048
C090519	L1-L2	IV	AR	Body	No Load	Upper	-3.0861	3.0861	0.5835	-3.1856	0.5856	0.9078
C090519	L1-L2	IV	AR	Body	No Load	Lower	-3.0861	3.0861	0.6131	-0.9866	0.5226	2.6435
C090519	L1-L2	IV	AR	Room	No Load	Upper	-2.2967	2.2967	0.4912	-1.6792	0.5281	0.1576
C090519	L1-L2	IV	AR	Room	No Load	Lower	-2.2967	2.2967	0.6909	-0.2934	0.3866	1.6168
C090519	L1-L2	IV	FE	Body	Load	Upper	-5.6571	5.6571	0.4613	0.2503	3.2145	0.3260
C090519	L1-L2	IV	FE	Body	Load	Lower	-5.6571	5.6571	3.3755	0.9923	0.5044	1.8728
C090519	L1-L2	IV	FE	Room	Load	Upper	-4.8234	4.8234	3.3960	0.8097	0.5060	1.0040
C090519	L1-L2	IV	FE	Room	Load	Lower	-4.8234	4.8234	3.0228	1.6239	0.5265	2.3247
C090519	L1-L2	IV	FE	Body	No Load	Upper	-6.6237	6.6237	0.3422	-0.9365	1.4572	1.0464
C090519	L1-L2	IV	FE	Body	No Load	Lower	-6.6237	6.6237	1.6384	1.1621	0.3342	1.6096
C090519	L1-L2	IV	FE	Room	No Load	Upper	-5.5279	5.5279	0.3952	-0.2687	1.8314	1.0230
C090519	L1-L2	IV	FE	Room	No Load	Lower	-5.5279	5.5279	1.8885	1.4150	0.4441	1.6784
C090519	L1-L2	IV	LB	Body	Load	Upper	-5.2546	5.2546	0.5416	-1.6394	0.4188	-0.6904
C090519	L1-L2	IV	LB	Body	Load	Lower	-5.2546	5.2546	0.6338	0.0129	0.3879	1.6789
C090519	L1-L2	IV	LB	Room	Load	Upper	-3.9151	3.9151	0.3784	-1.7881	0.6928	-0.4267
C090519	L1-L2	IV	LB	Room	Load	Lower	-3.9151	3.9151	0.3502	0.5819	0.7680	1.0493
C090519	L1-L2	IV	LB	Body	No Load	Upper	-	-	-	-	-	-
C090519	L1-L2	IV	LB	Body	No Load	Lower	-	-	-	-	-	-
C090519	L1-L2	IV	LB	Room	No Load	Upper	-5.5399	5.5399	0.3678	-1.1748	1.0192	-0.0448
C090519	L1-L2	IV	LB	Room	No Load	Lower	-5.5399	5.5399	0.9961	0.2597	0.3715	1.1148

Table A.5: List of DIP-Boltzmann parameters for spine C090519, segment L3-L4.

Spine	Segment	Grade	Direction	Temp	Load	Curve	A	B	α_1	m_1	α_2	m_2
C090519	L3-L4	V	AR	Body	Load	Upper	-4.0667	4.0667	0.5229	-1.7426	0.5111	0.9472
C090519	L3-L4	V	AR	Body	Load	Lower	-4.0667	4.0667	0.6216	-1.1999	0.5617	2.8753
C090519	L3-L4	V	AR	Room	Load	Upper	-4.0926	4.0926	0.5200	-2.1202	0.6176	1.6338
C090519	L3-L4	V	AR	Room	Load	Lower	-4.0926	4.0926	0.5619	-1.1166	0.5497	2.4134
C090519	L3-L4	V	AR	Body	No Load	Upper	-5.7512	5.7512	0.3257	-1.3425	2.8046	0.0443
C090519	L3-L4	V	AR	Body	No Load	Lower	-5.7512	5.7512	2.5047	0.2739	0.3738	1.5638
C090519	L3-L4	V	AR	Room	No Load	Upper	-5.5602	5.5602	0.4525	-0.2964	3.5625	-0.0966
C090519	L3-L4	V	AR	Room	No Load	Lower	-5.5602	5.5602	3.3348	0.1031	0.4480	1.2681
C090519	L3-L4	V	FE	Body	Load	Upper	-4.9470	4.9470	0.8822	-1.2258	0.3795	0.8004
C090519	L3-L4	V	FE	Body	Load	Lower	-4.9470	4.9470	0.4210	2.3651	1.6605	2.3656
C090519	L3-L4	V	FE	Room	Load	Upper	-4.5793	4.5793	0.4576	-0.2909	1.0306	-0.0152
C090519	L3-L4	V	FE	Room	Load	Lower	-4.5793	4.5793	1.9859	1.4996	0.4806	1.5469
C090519	L3-L4	V	FE	Body	No Load	Upper	-6.2745	6.2745	0.4113	-0.8932	2.0129	0.2967
C090519	L3-L4	V	FE	Body	No Load	Lower	-6.2745	6.2745	2.0512	0.3803	0.4388	1.5287
C090519	L3-L4	V	FE	Room	No Load	Upper	-5.3365	5.3365	0.4949	-0.6314	2.6384	0.1765
C090519	L3-L4	V	FE	Room	No Load	Lower	-5.3365	5.3365	2.7592	0.4432	0.5387	0.8914
C090519	L3-L4	V	LB	Body	Load	Upper	-3.3101	3.3101	0.8023	-4.7351	0.5643	2.4530
C090519	L3-L4	V	LB	Body	Load	Lower	-3.3101	3.3101	0.6641	-2.7982	0.7739	4.8591
C090519	L3-L4	V	LB	Room	Load	Upper	-3.4444	3.4444	0.9830	-4.9085	0.6125	1.2837
C090519	L3-L4	V	LB	Room	Load	Lower	-3.4444	3.4444	0.8354	-3.1768	0.6293	3.2400
C090519	L3-L4	V	LB	Body	No Load	Upper	-8.6241	8.6241	0.4234	-1.3259	1.0028	-0.2816
C090519	L3-L4	V	LB	Body	No Load	Lower	-8.6241	8.6241	1.1571	-0.7781	0.5319	3.3533
C090519	L3-L4	V	LB	Room	No Load	Upper	-6.9020	6.9020	0.4280	-1.0223	1.6297	0.2890
C090519	L3-L4	V	LB	Room	No Load	Lower	-6.9020	6.9020	1.4363	0.2290	0.4362	1.2136

Table A.6: List of DIP-Boltzmann parameters for spine C090519, segment L5-S1.

Spine	Segment	Grade	Direction	Temp	Load	Curve	A	B	α_1	m_1	α_2	m_2
C090519	L5-S1	V	AR	Body	Load	Upper	-1.8729	1.8729	0.7375	-3.9529	0.7012	1.8309
C090519	L5-S1	V	AR	Body	Load	Lower	-1.8729	1.8729	0.5598	-2.2054	0.7982	4.5955
C090519	L5-S1	V	AR	Room	Load	Upper	-1.7260	1.7260	0.6058	-3.5286	0.8353	2.6923
C090519	L5-S1	V	AR	Room	Load	Lower	-1.7260	1.7260	0.5429	-1.7734	0.8047	4.1707
C090519	L5-S1	V	AR	Body	No Load	Upper	-3.7587	3.7587	0.3762	-0.9755	1.3057	0.2378
C090519	L5-S1	V	AR	Body	No Load	Lower	-3.7587	3.75876	1.0534	0.0506	0.4419	2.3228
C090519	L5-S1	V	AR	Room	No Load	Upper	-2.8217	2.8217	0.3781	-0.3305	2.0488	-0.1025
C090519	L5-S1	V	AR	Room	No Load	Lower	-2.8217	2.8217	2.1368	0.1834	0.4084	1.6067
C090519	L5-S1	V	FE	Body	Load	Upper	-5.2851	5.2851	0.9066	-2.3624	0.4672	1.5738
C090519	L5-S1	V	FE	Body	Load	Lower	-5.2851	5.2851	0.8143	-0.3078	0.5720	3.7914
C090519	L5-S1	V	FE	Room	Load	Upper	-4.0241	4.0241	0.4226	-0.0767	0.7495	0.0432
C090519	L5-S1	V	FE	Room	Load	Lower	-4.0241	4.0241	0.4513	2.1238	0.7007	2.142
C090519	L5-S1	V	FE	Body	No Load	Upper	-7.0376	7.0376	0.5181	-1.8353	0.8605	0.6508
C090519	L5-S1	V	FE	Body	No Load	Lower	-7.0376	7.0376	1.1068	0.2695	0.4449	1.0918
C090519	L5-S1	V	FE	Room	No Load	Upper	-5.8044	5.8044	0.5164	-1.3017	1.8564	0.7694
C090519	L5-S1	V	FE	Room	No Load	Lower	-5.8044	5.8044	0.4814	0.8688	2.2282	1.0124
C090519	L5-S1	V	LB	Body	Load	Upper	-1.7586	1.7586	0.8368	-4.9331	0.5331	1.0825
C090519	L5-S1	V	LB	Body	Load	Lower	-1.7586	1.7586	0.6545	-2.7487	0.5971	4.1331
C090519	L5-S1	V	LB	Room	Load	Upper	-0.7855	0.7855	1.1110	-5.7002	0.4956	0.5615
C090519	L5-S1	V	LB	Room	Load	Lower	-0.7855	0.7855	0.7615	-4.0906	0.4815	2.9153
C090519	L5-S1	V	LB	Body	No Load	Upper	-4.9230	4.9230	0.5922	-2.1664	0.4283	0.7342
C090519	L5-S1	V	LB	Body	No Load	Lower	-4.9230	4.9230	0.8224	-1.4504	0.5913	3.8062
C090519	L5-S1	V	LB	Room	No Load	Upper	-2.1435	2.1435	0.7045	-2.9299	0.3295	2.2136
C090519	L5-S1	V	LB	Room	No Load	Lower	-2.1435	2.1435	0.7683	-1.9352	0.3689	4.0402

Table A.7: List of DIP-Boltzmann parameters for spine C091292, segment L1-L2.

Spine	Segment	Grade	Direction	Temp	Load	Curve	A	B	α_1	m_1	α_2	m_2
C091292	L1-L2	V	AR	Body	Load	Upper	-2.2471	2.2471	0.5754	-3.2741	0.5439	1.7406
C091292	L1-L2	V	AR	Body	Load	Lower	-2.2471	2.2471	0.5819	-1.4303	0.5744	3.6353
C091292	L1-L2	V	AR	Room	Load	Upper	-1.3537	1.3537	0.6349	-3.6311	0.6441	2.3190
C091292	L1-L2	V	AR	Room	Load	Lower	-1.3537	1.3537	0.5238	-2.1465	0.7076	3.8084
C091292	L1-L2	V	AR	Body	No Load	Upper	-3.3686	3.3686	0.4373	-1.9488	0.5579	0.0630
C091292	L1-L2	V	AR	Body	No Load	Lower	-3.3686	3.3686	0.7079	0.7208	0.3582	0.8570
C091292	L1-L2	V	AR	Room	No Load	Upper	-2.3289	2.3289	0.3627	-1.7911	0.6679	0.2677
C091292	L1-L2	V	AR	Room	No Load	Lower	-2.3289	2.3289	0.3773	0.4018	0.6707	1.6145
C091292	L1-L2	V	FE	Body	Load	Upper	-4.9492	4.9492	0.3419	-1.2532	1.8339	0.3746
C091292	L1-L2	V	FE	Body	Load	Lower	-4.9492	4.9492	2.2888	0.9594	0.3721	1.6808
C091292	L1-L2	V	FE	Room	Load	Upper	-4.0853	4.0853	0.3618	-0.1272	2.4831	0.9301
C091292	L1-L2	V	FE	Room	Load	Lower	-4.0853	4.0853	2.8617	1.5269	0.4623	2.3090
C091292	L1-L2	V	FE	Body	No Load	Upper	-5.5505	5.5505	0.4701	-2.2249	0.6968	0.9739
C091292	L1-L2	V	FE	Body	No Load	Lower	-5.5505	5.5505	0.6904	0.3176	0.4131	1.6814
C091292	L1-L2	V	FE	Room	No Load	Upper	-4.6440	4.6440	0.3522	-1.0292	0.6600	0.1789
C091292	L1-L2	V	FE	Room	No Load	Lower	-4.6440	4.6440	0.9309	0.0548	0.3647	2.5378
C091292	L1-L2	V	LB	Body	Load	Upper	-6.5866	6.5866	0.6485	-3.8642	0.8445	1.6610
C091292	L1-L2	V	LB	Body	Load	Lower	-6.5866	6.5866	0.5284	-1.7519	0.8047	3.4062
C091292	L1-L2	V	LB	Room	Load	Upper	-4.3861	4.3861	0.7026	-4.5342	0.6855	2.5978
C091292	L1-L2	V	LB	Room	Load	Lower	-4.3861	4.3861	0.5294	-2.3574	0.8207	4.6434
C091292	L1-L2	V	LB	Body	No Load	Upper	-7.5915	7.5915	0.4520	-1.9502	0.7570	0.8694
C091292	L1-L2	V	LB	Body	No Load	Lower	-7.5915	7.5915	0.5796	-0.4885	0.4958	2.1870
C091292	L1-L2	V	LB	Room	No Load	Upper	-6.8616	6.8616	0.5163	-2.3357	0.5888	1.2396
C091292	L1-L2	V	LB	Room	No Load	Lower	-6.8616	6.8616	0.6277	-1.2039	0.6011	3.2797

Table A.8: List of DIP-Boltzmann parameters for spine C091292, segment L3-L4.

Spine	Segment	Grade	Direction	Temp	Load	Curve	A	B	α_1	m_1	α_2	m_2
C091292	L3-L4	III	AR	Body	Load	Upper	-1.4681	1.4681	0.6160	-3.9699	0.6092	2.6922
C091292	L3-L4	III	AR	Body	Load	Lower	-1.4681	1.4681	0.5179	-1.9735	0.7753	4.6731
C091292	L3-L4	III	AR	Room	Load	Upper	-1.6261	1.6261	0.5574	-3.0322	0.5460	2.3686
C091292	L3-L4	III	AR	Room	Load	Lower	-1.6261	1.6261	0.5737	-1.6016	0.6605	4.2992
C091292	L3-L4	III	AR	Body	No Load	Upper	-2.8904	2.8904	0.3579	-1.1607	0.7821	0.4017
C091292	L3-L4	III	AR	Body	No Load	Lower	-2.8904	2.8904	0.5508	-0.1264	0.5559	2.0417
C091292	L3-L4	III	AR	Room	No Load	Upper	-3.7383	3.7383	0.3332	-0.6357	1.1480	-0.1299
C091292	L3-L4	III	AR	Room	No Load	Lower	-3.7383	3.7383	1.0514	0.2650	0.3748	1.8328
C091292	L3-L4	III	FE	Body	Load	Upper	-1.1950	1.1950	0.6954	-4.4980	0.5669	2.4928
C091292	L3-L4	III	FE	Body	Load	Lower	-1.1950	1.1950	0.5679	-2.2404	0.6657	4.5421
C091292	L3-L4	III	FE	Room	Load	Upper	-4.7284	4.7284	4.0797	0.0080	0.5175	0.2002
C091292	L3-L4	III	FE	Room	Load	Lower	-4.7284	4.7284	3.4093	0.5522	0.5473	1.7580
C091292	L3-L4	III	FE	Body	No Load	Upper	-6.4306	6.4306	0.4102	-0.0232	2.0377	0.8691
C091292	L3-L4	III	FE	Body	No Load	Lower	-6.4306	6.4306	1.7735	1.2247	0.4301	2.0750
C091292	L3-L4	III	FE	Room	No Load	Upper	-4.7087	4.7087	0.4288	0.4599	2.1468	0.7093
C091292	L3-L4	III	FE	Room	No Load	Lower	-4.7087	4.7087	2.0832	0.7785	0.4664	2.0039
C091292	L3-L4	III	LB	Body	Load	Upper	-5.9189	5.9189	0.7657	-4.9955	0.6300	1.2204
C091292	L3-L4	III	LB	Body	Load	Lower	-5.9189	5.9189	0.5857	-1.6483	0.7495	4.2996
C091292	L3-L4	III	LB	Room	Load	Upper	-9.1545	9.1545	1.1145	-5.3277	0.9628	-0.1610
C091292	L3-L4	III	LB	Room	Load	Lower	-9.1545	9.1545	0.6740	-3.1510	0.8713	1.7346
C091292	L3-L4	III	LB	Body	No Load	Upper	-13.3970	13.3970	0.4460	-1.0252	1.1632	-0.0439
C091292	L3-L4	III	LB	Body	No Load	Lower	-13.3970	13.3970	1.1231	-0.1193	0.4628	1.3451
C091292	L3-L4	III	LB	Room	No Load	Upper	-9.3252	9.3252	0.4724	-0.8740	0.8968	0.4225
C091292	L3-L4	III	LB	Room	No Load	Lower	-9.3252	9.3252	0.8257	0.2775	0.4930	2.0862

Table A.9: List of DIP-Boltzmann parameters for spine C091292, segment L5-S1.

Spine	Segment	Grade	Direction	Temp	Load	Curve	A	B	α_1	m_1	α_2	m_2
C091292	L5-S1	V	AR	Body	Load	Upper	-1.6237	1.6237	0.5547	-3.9172	0.7157	4.0107
C091292	L5-S1	V	AR	Body	Load	Lower	-1.6237	1.6237	0.4864	-2.0981	0.8928	5.2044
C091292	L5-S1	V	AR	Room	Load	Upper	-0.6981	0.6981	0.6128	-4.0205	0.5979	3.3205
C091292	L5-S1	V	AR	Room	Load	Lower	-0.6981	0.6981	0.5712	-2.7138	0.6656	4.5731
C091292	L5-S1	V	AR	Body	No Load	Upper	-3.2640	3.2640	0.3768	-1.7677	0.7790	0.3465
C091292	L5-S1	V	AR	Body	No Load	Lower	-3.2640	3.2640	0.7332	0.4446	0.3680	1.1904
C091292	L5-S1	V	AR	Room	No Load	Upper	-1.7128	1.7128	0.4937	-3.5978	0.6490	2.0415
C091292	L5-S1	V	AR	Room	No Load	Lower	-1.7128	1.7128	0.4632	-1.7482	0.5524	2.6945
C091292	L5-S1	V	FE	Body	Load	Upper	-8.6020	8.6020	0.8028	-0.5641	8.2776	-0.2791
C091292	L5-S1	V	FE	Body	Load	Lower	-8.6020	8.6020	0.6780	1.3715	5.7536	1.4331
C091292	L5-S1	V	FE	Room	Load	Upper	-8.1236	8.1236	5.5978	-1.6242	0.7109	-1.2340
C091292	L5-S1	V	FE	Room	Load	Lower	-8.1236	8.1236	4.8267	0.5896	0.6551	0.7393
C091292	L5-S1	V	FE	Body	No Load	Upper	-10.4762	10.4762	0.4940	-0.8759	1.5316	1.0228
C091292	L5-S1	V	FE	Body	No Load	Lower	-10.4762	10.4762	1.4538	1.3262	0.5053	1.3891
C091292	L5-S1	V	FE	Room	No Load	Upper	-8.9391	8.9391	0.4843	-0.4606	1.7043	0.7243
C091292	L5-S1	V	FE	Room	No Load	Lower	-8.9391	8.9391	0.5084	1.4226	1.5603	1.5749
C091292	L5-S1	V	LB	Body	Load	Upper	-1.6748	1.6748	0.7349	-4.6766	0.5621	1.6398
C091292	L5-S1	V	LB	Body	Load	Lower	-1.6748	1.6748	0.5927	-2.1584	0.6032	4.1475
C091292	L5-S1	V	LB	Room	Load	Upper	-1.0406	1.0406	0.7976	-4.8077	0.6208	1.3716
C091292	L5-S1	V	LB	Room	Load	Lower	-1.0406	1.0406	0.6220	-2.2010	0.6734	4.4038
C091292	L5-S1	V	LB	Body	No Load	Upper	-6.9617	6.9617	0.4889	-2.0198	0.6166	0.7805
C091292	L5-S1	V	LB	Body	No Load	Lower	-6.9617	6.9617	0.6965	-0.4548	0.4699	2.3033
C091292	L5-S1	V	LB	Room	No Load	Upper	-4.9999	4.9999	0.3651	-1.4849	0.6871	0.2327
C091292	L5-S1	V	LB	Room	No Load	Lower	-4.9999	4.9999	0.6247	-0.0059	0.4040	1.9725

Table A.10: List of DIP-Boltzmann parameters for spine C091351, segment L1-L2.

Spine	Segment	Grade	Direction	Temp	Load	Curve	A	B	α_1	m_1	α_2	m_2
C091351	L1-L2	II	AR	Body	Load	Upper	-2.4579	2.4579	0.5953	-3.5006	0.5138	1.6986
C091351	L1-L2	II	AR	Body	Load	Lower	-2.4579	2.4579	0.6150	-2.4064	0.5959	3.5716
C091351	L1-L2	II	AR	Room	Load	Upper	-1.7510	1.7510	0.6127	-3.4946	0.5478	2.1993
C091351	L1-L2	II	AR	Room	Load	Lower	-1.7510	1.7510	0.5916	-2.3269	0.5673	3.4602
C091351	L1-L2	II	AR	Body	No Load	Upper	-3.8007	3.8007	0.3323	-1.1587	1.1324	-0.4641
C091351	L1-L2	II	AR	Body	No Load	Lower	-3.8007	3.8007	1.2224	-0.0274	0.3400	1.1321
C091351	L1-L2	II	AR	Room	No Load	Upper	-2.6320	2.6320	0.3671	-0.6957	0.9699	-0.2724
C091351	L1-L2	II	AR	Room	No Load	Lower	-2.6320	2.6320	0.9774	0.2189	0.3680	0.7292
C091351	L1-L2	II	FE	Body	Load	Upper	-5.3069	5.3069	3.5463	1.1424	0.5556	1.1998
C091351	L1-L2	II	FE	Body	Load	Lower	-5.3069	5.3069	3.1934	1.6843	0.6298	2.5219
C091351	L1-L2	II	FE	Room	Load	Upper	-4.4986	4.4986	0.5629	1.0898	2.7139	1.2866
C091351	L1-L2	II	FE	Room	Load	Lower	-4.4986	4.4986	2.8467	2.1055	0.6002	2.3648
C091351	L1-L2	II	FE	Body	No Load	Upper	-6.0386	6.0386	0.4291	0.1479	1.6463	1.4092
C091351	L1-L2	II	FE	Body	No Load	Lower	-6.0386	6.0386	1.4840	1.4378	0.4923	2.0425
C091351	L1-L2	II	FE	Room	No Load	Upper	-4.4620	4.4620	0.4523	0.4742	1.4578	1.1715
C091351	L1-L2	II	FE	Room	No Load	Lower	-4.4620	4.4620	1.4283	1.1424	0.5088	1.8999
C091351	L1-L2	II	LB	Body	Load	Upper	-6.4253	6.4253	0.9202	-1.3815	0.3495	-0.3793
C091351	L1-L2	II	LB	Body	Load	Lower	-6.4253	6.4253	1.3223	0.1607	0.3651	2.4054
C091351	L1-L2	II	LB	Room	Load	Upper	-4.4735	4.4735	1.0952	-3.4695	0.4010	-0.3099
C091351	L1-L2	II	LB	Room	Load	Lower	-4.4735	4.4735	1.0741	-1.5019	0.3944	1.7750
C091351	L1-L2	II	LB	Body	No Load	Upper	-8.4727	8.4727	0.3618	-1.1022	0.8446	0.2922
C091351	L1-L2	II	LB	Body	No Load	Lower	-8.4727	8.4727	0.7603	-0.3034	0.4275	2.5324
C091351	L1-L2	II	LB	Room	No Load	Upper	-6.0181	6.0181	0.3716	-1.1680	1.2354	0.3770
C091351	L1-L2	II	LB	Room	No Load	Lower	-6.0181	6.0181	1.2232	0.2189	0.3607	0.8474

Table A.11: List of DIP-Boltzmann parameters for spine C091351, segment L3-L4.

Spine	Segment	Grade	Direction	Temp	Load	Curve	A	B	α_1	m_1	α_2	m_2
C091351	L3-L4	III	AR	Body	Load	Upper	-3.1836	3.1836	0.4561	-1.8469	0.5312	0.5004
C091351	L3-L4	III	AR	Body	Load	Lower	-3.1836	3.1836	0.5299	0.0364	0.4389	1.3700
C091351	L3-L4	III	AR	Room	Load	Upper	-	-	-	-	-	-
C091351	L3-L4	III	AR	Room	Load	Lower	-	-	-	-	-	-
C091351	L3-L4	III	AR	Body	No Load	Upper	-4.8695	4.8695	0.4067	-0.8371	3.2954	-0.0371
C091351	L3-L4	III	AR	Body	No Load	Lower	-4.8695	4.8695	3.0822	0.0518	0.4211	1.3326
C091351	L3-L4	III	AR	Room	No Load	Upper	-	-	-	-	-	-
C091351	L3-L4	III	AR	Room	No Load	Lower	-	-	-	-	-	-
C091351	L3-L4	III	FE	Body	Load	Upper	-8.5484	8.5484	0.8130	1.2500	3.9554	1.4704
C091351	L3-L4	III	FE	Body	Load	Lower	-8.5484	8.5484	4.0059	2.0096	0.9409	2.7128
C091351	L3-L4	III	FE	Room	Load	Upper	-7.8188	7.8188	0.7524	0.3652	9.1361	0.4203
C091351	L3-L4	III	FE	Room	Load	Lower	-7.8188	7.8188	10.5426	1.0427	1.01175	1.5349
C091351	L3-L4	III	FE	Body	No Load	Upper	-8.3324	8.3324	0.4973	0.6747	1.2315	1.3352
C091351	L3-L4	III	FE	Body	No Load	Lower	-8.3324	8.3324	1.3333	0.8917	0.5968	2.7717
C091351	L3-L4	III	FE	Room	No Load	Upper	-8.2981	8.2981	0.4581	0.4218	1.5874	1.6066
C091351	L3-L4	III	FE	Room	No Load	Lower	-8.2981	8.2981	1.4641	1.4357	0.5730	2.3676
C091351	L3-L4	III	LB	Body	Load	Upper	-7.4101	7.4101	0.4462	-1.6105	0.7403	0.0872
C091351	L3-L4	III	LB	Body	Load	Lower	-7.4101	7.4101	0.4377	0.3830	0.6686	2.0560
C091351	L3-L4	III	LB	Room	Load	Upper	-7.8880	7.8880	0.3280	-1.2808	1.6067	0.3414
C091351	L3-L4	III	LB	Room	Load	Lower	-7.8880	7.8880	0.3205	0.6549	1.4701	1.5039
C091351	L3-L4	III	LB	Body	No Load	Upper	-9.4737	9.4737	0.3968	-1.2207	1.0092	0.6507
C091351	L3-L4	III	LB	Body	No Load	Lower	-9.4737	9.4737	0.4062	0.9246	0.8731	1.0770
C091351	L3-L4	III	LB	Room	No Load	Upper	-9.1278	9.1278	0.4333	-0.4884	1.8089	0.6374
C091351	L3-L4	III	LB	Room	No Load	Lower	-9.1278	9.1278	0.4303	0.7458	1.6365	0.8537

Table A.12: List of DIP-Boltzmann parameters for spine C091351, segment L5-S1.

Spine	Segment	Grade	Direction	Temp	Load	Curve	A	B	α_1	m_1	α_2	m_2
C091351	L5-S1	III	AR	Body	Load	Upper	-1.5114	1.5114	0.7832	-3.7441	0.5435	2.7956
C091351	L5-S1	III	AR	Body	Load	Lower	-1.5114	1.5114	0.4058	-2.4028	0.4767	4.0392
C091351	L5-S1	III	AR	Room	Load	Upper	-0.9789	0.9789	0.7840	-4.5118	0.6322	2.8041
C091351	L5-S1	III	AR	Room	Load	Lower	-0.9789	0.9789	0.6725	-2.0425	0.8192	4.2985
C091351	L5-S1	III	AR	Body	No Load	Upper	-2.5971	2.5971	0.5350	-1.3334	0.4758	0.1513
C091351	L5-S1	III	AR	Body	No Load	Lower	-2.5971	2.5971	0.5592	-0.6371	0.4912	1.5920
C091351	L5-S1	III	AR	Room	No Load	Upper	-1.7083	1.7083	0.5376	-2.9466	0.4935	1.2857
C091351	L5-S1	III	AR	Room	No Load	Lower	-1.7083	1.7083	0.6300	-1.4571	0.5569	2.8210
C091351	L5-S1	III	FE	Body	Load	Upper	-8.3983	8.3983	2.1991	1.2960	0.6196	1.3195
C091351	L5-S1	III	FE	Body	Load	Lower	-8.3983	8.3983	1.6362	2.0141	0.6756	2.8493
C091351	L5-S1	III	FE	Room	Load	Upper	-8.1394	8.1394	4.7893	0.1228	0.7962	0.1895
C091351	L5-S1	III	FE	Room	Load	Lower	-8.1394	8.1394	9.7580	1.3541	1.1648	1.4063
C091351	L5-S1	III	FE	Body	No Load	Upper	-9.2361	9.2361	0.5102	0.8893	1.2882	1.2129
C091351	L5-S1	III	FE	Body	No Load	Lower	-9.2361	9.2361	1.2040	0.6952	0.6854	2.7474
C091351	L5-S1	III	FE	Room	No Load	Upper	-8.3628	8.3628	0.4289	-0.7764	1.5508	1.0897
C091351	L5-S1	III	FE	Room	No Load	Lower	-8.3628	8.3628	1.4281	1.0554	0.4690	1.3409
C091351	L5-S1	III	LB	Body	Load	Upper	-	-	-	-	-	-
C091351	L5-S1	III	LB	Body	Load	Lower	-	-	-	-	-	-
C091351	L5-S1	III	LB	Room	Load	Upper	-2.4049	2.4049	0.4244	-2.2073	0.5238	1.5996
C091351	L5-S1	III	LB	Room	Load	Lower	-2.4049	2.4049	0.5103	-1.4383	0.5822	4.1267
C091351	L5-S1	III	LB	Body	No Load	Upper	-6.2559	6.2559	0.3835	-1.0154	1.5105	-0.2433
C091351	L5-S1	III	LB	Body	No Load	Lower	-6.2559	6.2559	1.4416	-0.4525	0.4190	1.8080
C091351	L5-S1	III	LB	Room	No Load	Upper	-5.3507	5.3507	0.4523	-1.0511	1.8960	-0.3192
C091351	L5-S1	III	LB	Room	No Load	Lower	-5.3507	5.3507	1.8350	-0.4905	0.4158	1.7531

Table A.13: List of DIP-Boltzmann parameters for spine C100115, segment L2-L3.

Spine	Segment	Grade	Direction	Temp	Load	Curve	A	B	α_1	m_1	α_2	m_2
C100115	L2-L3	II	AR	Body	Load	Upper	-1.4646	1.4646	0.5440	-3.6709	0.4406	4.1625
C100115	L2-L3	II	AR	Body	Load	Lower	-1.4646	1.4646	0.4667	-2.6250	0.5483	4.8654
C100115	L2-L3	II	AR	Room	Load	Upper	-1.0159	1.0159	0.6268	-3.7032	0.5663	3.6008
C100115	L2-L3	II	AR	Room	Load	Lower	-1.0159	1.0159	0.5686	-2.9827	0.6355	4.2317
C100115	L2-L3	II	FE	Body	Load	Upper	-7.0442	7.0442	0.4889	-0.3595	6.3114	-0.4704
C100115	L2-L3	II	FE	Body	Load	Lower	-7.0442	7.0442	3.4230	0.1753	0.5328	2.0639
C100115	L2-L3	II	FE	Room	Load	Upper	-6.2426	6.2426	5.2863	-0.1263	0.6866	1.0869
C100115	L2-L3	II	FE	Room	Load	Lower	-6.2426	6.2426	7.5186	0.2298	0.8321	1.7887
C100115	L2-L3	II	LB	Body	Load	Upper	-11.0840	11.0840	0.4914	-1.1272	7.6871	-0.8252
C100115	L2-L3	II	LB	Body	Load	Lower	-11.0840	11.0840	7.4433	0.2187	0.4658	1.3391
C100115	L2-L3	II	LB	Room	Load	Upper	-8.3789	8.3789	0.4583	-0.2652	2.2639	0.4673
C100115	L2-L3	II	LB	Room	Load	Lower	-8.3789	8.3789	3.0024	1.3314	0.4481	1.3449

Table A.14: List of DIP-Boltzmann parameters for spine C100115, segment L4-L5.

Spine	Segment	Grade	Direction	Temp	Load	Curve	A	B	α_1	m_1	α_2	m_2
C100115	L4-L5	II	AR	Body	Load	Upper	-2.3737	2.3737	0.5649	-4.1177	0.6754	3.7304
C100115	L4-L5	II	AR	Body	Load	Lower	-2.3737	2.3737	0.5020	-3.1838	0.6484	4.1233
C100115	L4-L5	II	AR	Room	Load	Upper	-2.3495	2.3495	0.5701	-4.1954	0.6935	3.6702
C100115	L4-L5	II	AR	Room	Load	Lower	-2.3495	2.3495	0.5233	-3.5869	0.6546	4.1235
C100115	L4-L5	II	FE	Body	Load	Upper	-9.4659	9.4659	0.4609	0.9403	1.7068	1.0422
C100115	L4-L5	II	FE	Body	Load	Lower	-9.4659	9.4659	1.4381	1.8607	0.5644	2.3713
C100115	L4-L5	II	FE	Room	Load	Upper	-9.5881	9.5881	0.5012	0.9767	1.8150	1.0256
C100115	L4-L5	II	FE	Room	Load	Lower	-9.5881	9.5881	1.4978	1.5143	0.6042	2.5334
C100115	L4-L5	II	LB	Body	Load	Upper	-9.4818	9.4818	0.4065	-1.2917	2.0368	-0.4158
C100115	L4-L5	II	LB	Body	Load	Lower	-9.4818	9.4818	1.6727	1.3126	0.3750	1.5507
C100115	L4-L5	II	LB	Room	Load	Upper	-9.0474	9.0474	4.2121	-3.5212	0.5335	-2.4922
C100115	L4-L5	II	LB	Room	Load	Lower	-9.0474	9.0474	4.1464	-1.5037	0.4493	-0.5658

Table A.15: List of DIP-Boltzmann parameters for spine S090647, segment L4-L5.

Spine	Segment	Grade	Direction	Temp	Load	Curve	A	B	α_1	m_1	α_2	m_2
S090647	L4-L5	IV	AR	Body	Load	Upper	-4.0925	4.0925	0.7973	-3.6062	0.5374	2.3754
S090647	L4-L5	IV	AR	Body	Load	Lower	-4.0925	4.0925	0.7394	-2.3315	0.6556	3.8460
S090647	L4-L5	IV	AR	Room	Load	Upper	-3.2457	3.2457	0.4961	-2.9025	0.7484	2.4627
S090647	L4-L5	IV	AR	Room	Load	Lower	-3.2457	3.2457	0.4168	-1.3284	0.7404	3.3776
S090647	L4-L5	IV	FE	Body	Load	Upper	-1.9768	1.9768	0.9244	-6.0163	0.4957	2.4398
S090647	L4-L5	IV	FE	Body	Load	Lower	-1.9768	1.9768	0.4556	-3.9217	0.6761	4.9197
S090647	L4-L5	IV	FE	Room	Load	Upper	-5.0410	5.0410	0.4153	0.8590	1.4640	1.6292
S090647	L4-L5	IV	FE	Room	Load	Lower	-5.0410	5.0410	0.4968	2.8370	1.8398	2.8389
S090647	L4-L5	IV	LB	Body	Load	Upper	-7.9447	7.9447	0.6214	-4.0002	0.8972	2.7551
S090647	L4-L5	IV	LB	Body	Load	Lower	-7.9447	7.9447	0.4666	-1.3088	1.1240	5.0682
S090647	L4-L5	IV	LB	Room	Load	Upper	-7.0558	7.0558	0.6171	-4.0452	0.5698	2.2198
S090647	L4-L5	IV	LB	Room	Load	Lower	-7.0558	7.0558	0.5547	-2.2136	0.6980	4.4180

Table A.16: List of DIP-Boltzmann parameters for spine S091199, segment L1-L2.

Spine	Segment	Grade	Direction	Temp	Load	Curve	A	B	α_1	m_1	α_2	m_2
S091199	L1-L2	V	AR	Body	Load	Upper	-3.0265	3.0265	0.8874	-4.1836	0.4506	-0.4313
S091199	L1-L2	V	AR	Body	Load	Lower	-3.0265	3.0265	0.8808	-2.7561	0.4348	1.5263
S091199	L1-L2	V	AR	Room	Load	Upper	-2.6610	2.6610	0.7849	-3.2613	0.4340	-0.4673
S091199	L1-L2	V	AR	Room	Load	Lower	-2.6610	2.6610	0.9121	-1.6090	0.4163	1.4612
S091199	L1-L2	V	AR	Body	No Load	Upper	-4.2341	4.2341	0.4471	-1.6783	2.5319	-0.4015
S091199	L1-L2	V	AR	Body	No Load	Lower	-4.2341	4.2341	3.1308	-0.0723	0.4107	0.4699
S091199	L1-L2	V	AR	Room	No Load	Upper	-3.9000	3.9000	0.4429	-1.3448	2.5248	-0.2641
S091199	L1-L2	V	AR	Room	No Load	Lower	-3.9000	3.9000	2.8727	0.0950	0.4505	0.9672
S091199	L1-L2	V	FE	Body	Load	Upper	-3.6613	3.6613	0.3645	-0.2873	1.3156	3.0946
S091199	L1-L2	V	FE	Body	Load	Lower	-3.6613	3.6613	0.4728	2.4882	1.5106	4.3614
S091199	L1-L2	V	FE	Room	Load	Upper	-2.8643	2.8643	0.3862	0.1932	2.3316	0.2745
S091199	L1-L2	V	FE	Room	Load	Lower	-2.8643	2.8643	1.7533	1.4619	0.4714	2.1322
S091199	L1-L2	V	FE	Body	No Load	Upper	-5.5569	5.5569	0.4164	-0.9946	1.5406	0.3645
S091199	L1-L2	V	FE	Body	No Load	Lower	-5.5569	5.5569	1.8119	0.4774	0.4326	1.8521
S091199	L1-L2	V	FE	Room	No Load	Upper	-3.5987	3.5987	0.4629	-1.8843	0.6768	1.1771
S091199	L1-L2	V	FE	Room	No Load	Lower	-3.5987	3.5987	0.7805	-0.1960	0.6007	3.3841
S091199	L1-L2	V	LB	Body	Load	Upper	-1.5598	1.5598	0.6463	-4.5532	0.5370	2.6141
S091199	L1-L2	V	LB	Body	Load	Lower	-1.5598	1.5598	0.5255	-1.9824	0.7308	4.9537
S091199	L1-L2	V	LB	Room	Load	Upper	-1.9610	1.9610	0.5859	-4.4903	0.5996	3.3163
S091199	L1-L2	V	LB	Room	Load	Lower	-1.9610	1.9610	0.5129	-1.6924	0.9441	5.8383
S091199	L1-L2	V	LB	Body	No Load	Upper	-5.7050	5.7050	0.3924	-1.4559	1.2314	0.9785
S091199	L1-L2	V	LB	Body	No Load	Lower	-5.7050	5.7050	0.3314	0.3392	1.1260	0.8511
S091199	L1-L2	V	LB	Room	No Load	Upper	-5.0285	5.0285	0.3786	-1.0299	1.1000	0.9854
S091199	L1-L2	V	LB	Room	No Load	Lower	-5.0285	5.0285	0.4623	1.0479	0.7043	2.9264

Table A.17: List of DIP-Boltzmann parameters for spine S091199, segment L3-L4.

Spine	Segment	Grade	Direction	Temp	Load	Curve	A	B	α_1	m_1	α_2	m_2
S091199	L3-L4	I	AR	Body	Load	Upper	-1.2112	1.2112	0.5949	-3.9580	0.5702	2.7082
S091199	L3-L4	I	AR	Body	Load	Lower	-1.2112	1.2112	0.4626	-1.1869	0.7236	4.4502
S091199	L3-L4	I	AR	Room	Load	Upper	-0.9305	0.9305	0.4945	-2.7124	0.6013	3.5392
S091199	L3-L4	I	AR	Room	Load	Lower	-0.9305	0.9305	0.4735	-1.6967	0.7043	4.3820
S091199	L3-L4	I	FE	Body	Load	Upper	-2.4105	2.4105	0.3611	-1.9276	2.1458	6.7191
S091199	L3-L4	I	FE	Body	Load	Lower	-2.4105	2.4105	0.3316	1.0330	4.7075	6.8386
S091199	L3-L4	I	FE	Room	Load	Upper	-2.2778	2.2778	0.2932	1.2715	3.8932	6.6706
S091199	L3-L4	I	FE	Room	Load	Lower	-2.2778	2.2778	0.3330	3.2292	6.3059	6.8365
S091199	L3-L4	I	LB	Body	Load	Upper	-9.8998	9.8998	1.5573	0.2112	0.5454	-1.0109
S091199	L3-L4	I	LB	Body	Load	Lower	-9.8998	9.8998	1.6754	-0.1067	0.5645	1.2317
S091199	L3-L4	I	LB	Room	Load	Upper	-7.8977	7.8977	0.9326	-3.0940	0.8682	1.3143
S091199	L3-L4	I	LB	Room	Load	Lower	-7.8977	7.8977	1.1105	-1.7108	0.8170	3.6381

Table A.18: List of DIP-Boltzmann parameters for spine S091199, segment L5-S1.

Spine	Segment	Grade	Direction	Temp	Load	Curve	A	B	α_1	m_1	α_2	m_2
S091199	L5-S1	IV	AR	Body	Load	Upper	-1.1579	1.1579	0.4932	-2.1101	0.6318	2.0626
S091199	L5-S1	IV	AR	Body	Load	Lower	-1.1579	1.1579	0.6877	-0.4354	0.7469	4.4947
S091199	L5-S1	IV	AR	Room	Load	Upper	-0.9829	0.9829	0.4162	-1.8105	0.6779	2.9360
S091199	L5-S1	IV	AR	Room	Load	Lower	-0.9829	0.9829	0.5380	-0.0717	0.6579	4.3245
S091199	L5-S1	IV	AR	Body	No Load	Upper	-2.3292	2.3292	0.3474	-1.2119	0.7567	0.0988
S091199	L5-S1	IV	AR	Body	No Load	Lower	-2.3292	2.3292	0.7501	-0.6611	0.5489	3.0642
S091199	L5-S1	IV	AR	Room	No Load	Upper	-2.3143	2.3143	0.3498	-2.0846	0.7086	0.5994
S091199	L5-S1	IV	AR	Room	No Load	Lower	-2.3143	2.3143	0.3265	0.0127	0.7466	0.8638
S091199	L5-S1	IV	FE	Body	Load	Upper	-5.8441	5.8441	0.3880	-0.6356	1.0823	1.5880
S091199	L5-S1	IV	FE	Body	Load	Lower	-5.8441	5.8441	0.4083	1.9684	0.9579	2.5063
S091199	L5-S1	IV	FE	Room	Load	Upper	-3.5349	3.5349	0.4356	-0.6785	1.1684	4.8598
S091199	L5-S1	IV	FE	Room	Load	Lower	-3.5349	3.5349	0.3923	2.1200	1.7461	5.9483
S091199	L5-S1	IV	FE	Body	No Load	Upper	-8.5837	8.5837	0.4216	0.1308	1.2670	2.0351
S091199	L5-S1	IV	FE	Body	No Load	Lower	-8.5837	8.5837	0.8403	1.2051	0.5813	3.3437
S091199	L5-S1	IV	FE	Room	No Load	Upper	-8.4691	8.4691	0.4679	0.1216	1.2412	2.1537
S091199	L5-S1	IV	FE	Room	No Load	Lower	-8.4691	8.4691	0.7299	1.4216	0.6027	3.0082
S091199	L5-S1	IV	LB	Body	Load	Upper	-1.6633	1.6633	1.0974	-4.6453	0.4753	0.6243
S091199	L5-S1	IV	LB	Body	Load	Lower	-1.6633	1.6633	0.8495	-2.3456	0.5417	4.1382
S091199	L5-S1	IV	LB	Room	Load	Upper	-1.8520	1.8520	0.6503	-4.0596	0.6805	-0.2955
S091199	L5-S1	IV	LB	Room	Load	Lower	-1.8520	1.8520	0.6413	-0.8105	0.5050	2.3305
S091199	L5-S1	IV	LB	Body	No Load	Upper	-5.8774	5.8774	0.4129	-2.0671	1.0017	0.9929
S091199	L5-S1	IV	LB	Body	No Load	Lower	-5.8774	5.8774	1.1235	0.8437	0.3798	1.9113
S091199	L5-S1	IV	LB	Room	No Load	Upper	-4.4970	4.4970	0.6080	-1.0983	0.4392	-1.2952
S091199	L5-S1	IV	LB	Room	No Load	Lower	-4.4970	4.4970	1.1291	-0.4919	0.3921	1.5069

Table A.19: List of DIP-Boltzmann parameters for spine S100589, segment L1-L2.

Spine	Segment	Grade	Direction	Temp	Load	Curve	A	B	α_1	m_1	α_2	m_2
S100589	L1-L2	IV	AR	Body	Load	Upper	-4.2805	4.2805	0.7910	-1.5367	0.3532	-0.9314
S100589	L1-L2	IV	AR	Body	Load	Lower	-4.2805	4.2805	0.7929	-1.0835	0.3480	0.8214
S100589	L1-L2	IV	AR	Room	Load	Upper	-3.8811	3.8811	0.8995	-1.3447	0.3539	-0.7035
S100589	L1-L2	IV	AR	Room	Load	Lower	-3.8811	3.8811	0.9408	-0.9462	0.3550	1.1992
S100589	L1-L2	IV	AR	Body	No Load	Upper	-5.7348	5.7348	0.3655	-0.7401	3.0732	-0.3191
S100589	L1-L2	IV	AR	Body	No Load	Lower	-5.7348	5.7348	3.2417	-0.0661	0.3743	1.5563
S100589	L1-L2	IV	AR	Room	No Load	Upper	-5.0443	5.0443	0.3816	-0.7695	2.9635	-0.3390
S100589	L1-L2	IV	AR	Room	No Load	Lower	-5.0443	5.0443	3.1964	-0.0346	0.3771	1.3803
S100589	L1-L2	IV	FE	Body	Load	Upper	-6.5327	6.5327	0.4608	-1.7771	2.6846	0.6794
S100589	L1-L2	IV	FE	Body	Load	Lower	-6.5327	6.5327	0.4503	0.2452	2.9515	1.9094
S100589	L1-L2	IV	FE	Room	Load	Upper	-5.5334	5.5334	0.4579	-1.6268	2.4581	0.3545
S100589	L1-L2	IV	FE	Room	Load	Lower	-5.5334	5.5334	0.4607	0.2037	2.5714	1.5422
S100589	L1-L2	IV	FE	Body	No Load	Upper	-6.6663	6.6663	0.42869	-1.3912	1.7092	0.1150
S100589	L1-L2	IV	FE	Body	No Load	Lower	-6.6663	6.6663	1.8447	0.2103	0.4415	0.8334
S100589	L1-L2	IV	FE	Room	No Load	Upper	-5.9189	5.9189	0.4336	-1.2383	1.5965	0.1613
S100589	L1-L2	IV	FE	Room	No Load	Lower	-5.9189	5.9189	1.8701	0.3061	0.4325	1.0598
S100589	L1-L2	IV	LB	Body	Load	Upper	-5.5623	5.5623	0.3401	-1.8327	0.9678	-0.6688
S100589	L1-L2	IV	LB	Body	Load	Lower	-5.5623	5.5623	0.3276	0.8207	1.1425	1.0145
S100589	L1-L2	IV	LB	Room	Load	Upper	-4.9513	4.9513	0.3774	-1.8985	0.6257	0.4672
S100589	L1-L2	IV	LB	Room	Load	Lower	-4.9513	4.9513	0.4427	0.2580	0.5184	2.570
S100589	L1-L2	IV	LB	Body	No Load	Upper	-6.4356	6.4356	0.3500	-1.1738	1.4226	0.3237
S100589	L1-L2	IV	LB	Body	No Load	Lower	-6.4356	6.4356	1.4790	0.5078	0.3162	1.2191
S100589	L1-L2	IV	LB	Room	No Load	Upper	-6.8198	6.8198	0.3561	-1.1316	1.3431	-0.0462
S100589	L1-L2	IV	LB	Room	No Load	Lower	-6.8198	6.8198	1.4326	0.0879	0.3865	1.0966

Table A.20: List of DIP-Boltzmann parameters for spine S100589, segment L3-L4.

Spine	Segment	Grade	Direction	Temp	Load	Curve	A	B	α_1	m_1	α_2	m_2
S100589	L3-L4	IV	AR	Body	Load	Upper	-2.0507	2.0507	0.5480	-3.2361	0.6046	2.3827
S100589	L3-L4	IV	AR	Body	Load	Lower	-2.0507	2.0507	0.5375	-1.1819	0.6864	4.0879
S100589	L3-L4	IV	AR	Room	Load	Upper	-2.0945	2.0945	0.4980	-2.6869	0.5674	1.6801
S100589	L3-L4	IV	AR	Room	Load	Lower	-2.0945	2.0945	0.5400	-1.3732	0.6011	3.3656
S100589	L3-L4	IV	AR	Body	No Load	Upper	-2.8986	2.8986	0.4918	-2.8480	0.6013	1.1791
S100589	L3-L4	IV	AR	Body	No Load	Lower	-2.8986	2.8986	0.4710	0.2120	0.4741	1.6159
S100589	L3-L4	IV	AR	Room	No Load	Upper	-3.2415	3.2415	0.3416	-1.1785	1.0126	0.1343
S100589	L3-L4	IV	AR	Room	No Load	Lower	-3.2415	3.2415	0.3502	0.8459	0.9233	0.8611
S100589	L3-L4	IV	FE	Body	Load	Upper	-5.9064	5.9064	0.4397	0.8181	1.3718	1.7106
S100589	L3-L4	IV	FE	Body	Load	Lower	-5.9064	5.9064	0.5093	2.3898	1.2047	2.7402
S100589	L3-L4	IV	FE	Room	Load	Upper	-5.4739	5.4739	0.4859	0.6612	1.1419	1.7454
S100589	L3-L4	IV	FE	Room	Load	Lower	-5.4739	5.4739	0.5466	2.2949	1.1125	2.9593
S100589	L3-L4	IV	FE	Body	No Load	Upper	-6.6559	6.6559	0.4056	-0.1545	1.3323	1.4466
S100589	L3-L4	IV	FE	Body	No Load	Lower	-6.6559	6.6559	1.1669	1.4950	0.4421	2.3232
S100589	L3-L4	IV	FE	Room	No Load	Upper	-6.2121	6.2121	0.4363	0.0695	1.5168	1.2753
S100589	L3-L4	IV	FE	Room	No Load	Lower	-6.2121	6.2121	1.3626	1.4027	0.4830	2.2608
S100589	L3-L4	IV	LB	Body	Load	Upper	-3.7228	3.7228	0.6406	-4.1064	0.6681	2.8514
S100589	L3-L4	IV	LB	Body	Load	Lower	-3.7228	3.7228	0.5604	-1.6815	0.7656	4.8480
S100589	L3-L4	IV	LB	Room	Load	Upper	-3.9237	3.9237	0.6140	-4.2005	0.6445	2.7325
S100589	L3-L4	IV	LB	Room	Load	Lower	-3.9237	3.9237	0.5423	-1.8805	0.7482	4.5184
S100589	L3-L4	IV	LB	Body	No Load	Upper	-7.0932	7.0932	0.4597	-2.1902	0.7424	1.1019
S100589	L3-L4	IV	LB	Body	No Load	Lower	-7.0932	7.0932	0.5568	0.3098	0.4525	1.3207
S100589	L3-L4	IV	LB	Room	No Load	Upper	-6.4830	6.4830	0.4420	-1.7770	0.7889	0.9944
S100589	L3-L4	IV	LB	Room	No Load	Lower	-6.4830	6.4830	0.4531	0.7980	0.5971	1.0560

Table A.21: List of DIP-Boltzmann parameters for spine S100589, segment L5-S1.

Spine	Segment	Grade	Direction	Temp	Load	Curve	A	B	α_1	m_1	α_2	m_2
S100589	L5-S1	V	AR	Body	Load	Upper	-1.8271	1.8271	0.6385	-3.8064	0.6628	2.6365
S100589	L5-S1	V	AR	Body	Load	Lower	-1.8271	1.8271	0.5249	-1.1742	0.8283	4.5768
S100589	L5-S1	V	AR	Room	Load	Upper	-1.1916	1.1916	0.5652	-3.6936	0.6276	2.8661
S100589	L5-S1	V	AR	Room	Load	Lower	-1.1916	1.1916	0.5148	-1.7090	0.7357	4.4685
S100589	L5-S1	V	AR	Body	No Load	Upper	-3.4886	3.4886	0.4134	-1.9281	0.7296	0.3772
S100589	L5-S1	V	AR	Body	No Load	Lower	-3.4886	3.4886	0.7925	0.7634	0.3782	1.1572
S100589	L5-S1	V	AR	Room	No Load	Upper	-2.6625	2.6625	0.4033	-1.4264	0.7588	0.3191
S100589	L5-S1	V	AR	Room	No Load	Lower	-2.6625	2.6625	0.9164	0.5309	0.3882	1.3110
S100589	L5-S1	V	FE	Body	Load	Upper	-1.8408	1.8408	0.6873	-4.4884	0.5746	2.8305
S100589	L5-S1	V	FE	Body	Load	Lower	-1.8408	1.8408	0.5484	-2.4871	0.7292	5.0654
S100589	L5-S1	V	FE	Room	Load	Upper	-3.0582	3.0582	0.3884	-0.1515	1.4303	4.1638
S100589	L5-S1	V	FE	Room	Load	Lower	-3.0582	3.0582	0.4169	1.9349	1.7741	5.4740
S100589	L5-S1	V	FE	Body	No Load	Upper	-8.0186	8.0186	0.4082	-1.3108	1.6879	0.8537
S100589	L5-S1	V	FE	Body	No Load	Lower	-8.0186	8.0186	1.6376	0.8487	0.3934	1.2957
S100589	L5-S1	V	FE	Room	No Load	Upper	-5.6809	5.6809	0.5214	-2.4259	1.1931	1.2971
S100589	L5-S1	V	FE	Room	No Load	Lower	-5.6809	5.6809	1.2082	0.8357	0.4050	1.0820
S100589	L5-S1	V	LB	Body	Load	Upper	-1.1610	1.1610	0.7344	-4.8170	0.5624	2.2352
S100589	L5-S1	V	LB	Body	Load	Lower	-1.1610	1.1610	0.5945	-2.0781	0.6744	4.7587
S100589	L5-S1	V	LB	Room	Load	Upper	-0.7434	0.7434	0.7060	-4.6420	0.5766	2.7924
S100589	L5-S1	V	LB	Room	Load	Lower	-0.7434	0.7434	0.5791	-2.1175	0.7107	4.9375
S100589	L5-S1	V	LB	Body	No Load	Upper	-5.6136	5.6136	0.7921	-3.5960	0.5311	1.3537
S100589	L5-S1	V	LB	Body	No Load	Lower	-5.6136	5.6136	1.05576	-1.5994	0.5544	3.2605
S100589	L5-S1	V	LB	Room	No Load	Upper	-4.0898	4.0898	0.8567	-3.8877	0.6453	2.0492
S100589	L5-S1	V	LB	Room	No Load	Lower	-4.0898	4.0898	0.9019	-1.2955	0.5178	3.2413